Supplement of Biogeosciences, 23, 3855–3869, 2026
https://doi.org/10.5194/bg-23-3855-2026-supplement

Biogeosciences Open Access EGU

Supplement of

Bomb-radiocarbon signal suggests that soil carbon contributes to chlorophyll *a* in archival oak leaves

Naoto F. Ishikawa et al.

Correspondence to: Naoto F. Ishikawa (ishikawan@jamstec.go.jp)

S1. Purity Assessment

To identify and characterize impurity carbon in the purified Pheo *a* fractions, three additional assessments based on (i) diode array detector (DAD), (ii) Orbitrap MS, and (iii) GC/MS spectra were performed. Assessment (i) was subject to all eight samples, while assessment (ii) subject to 1952, 1968, 1973, 1982, and 1995 samples and assessment (iii) subject to 1952 and 1968 samples due to availability of leftover materials after CSRA.

(i) DAD spectrum

The DAD spectrum of all samples spanning from 300 to 720 nm absorbance was examined at the time window between 16.5 to 20.5 min when the Pheo *a* allomer, Pheo *a*, and Pheo *a* epimer were collected by fraction collector. The HPLC setting was the same as the second-step separation using Eclipse PAH column. Exogeneous compounds having absorbance at the 300–720 nm range were not found (Figure S3). Based on peak areas at 660 nm of Pheo *a* allomer, Pheo *a*, and Pheo *a* epimer, their relative proportion in each sample was estimated (Figure S4).

(ii) Orbitrap MS spectrum

Selected samples (1952, 1968, 1973, 1982, and 1995 CE) were injected to an UltiMate 3000 and Q Exactive™ Plus Hybrid Quadrupole-Orbitrap™ mass spectrometer (Thermo Fischer Scientific Inc., Waltham, MA, USA) using the electrospray ionization (ESI) method under an infusion mode. Exogeneous compounds that were ionized by ESI were not found except for Pheo *a* allomers (allomer 1: *m/z* 887.6, $C_{55}H_{74}N_4O_6$, allomer 2: *m/z* 903.6, $C_{55}H_{74}N_4O_7$, allomer 3: *m/z* 919.6, $C_{55}H_{74}N_4O_8$, allomer 4: *m/z* 935.6, $C_{55}H_{74}N_4O_9$) (Figure S5). The addition of oxygen to the Pheo *a* compound likely occurred in sample preparation and/or storage process due to an exposure to ambient air, which does not increase its C/N nor affect

sample purity for CSRA measurements. Based on peak areas at exact *m/z* of Pheo *a* and its allomers, their relative proportion in each sample was estimated (Figure S6). There was a strong positive correlation in proportions of Pheo *a* allomers between DAD-based estimates and Orbitrap MS-based estimates (Figure S7).

(iii) GC/MS spectrum

Selected samples (1952 and 1968 CE, 2.5 μgC and 3.8 μgC, respectively) were dissolved in *n*-hexane, and loaded on deactivated 1 % H_2O silica gel columns pre-conditioned with hexane. The N-1, N-2, and N-3 fractions were extracted with *n*-hexane, *n*-hexane/dichloromethane (50:50, v/v), and dichloromethane/methanol (90:10, v/v) respectively. N, O-bis(trimethylsilyl)trifluoroacetamide (BSTFA) was added to each vial and heated at 40 °C to derivatize the trimethylsilyl (TMS) ester. After drying with argon gas, these fractions were redissolved in 100 μL of *n*-hexane/dichloromethane and were injected (1 μL) to a gas chromatograph/mass spectrometer (GC/MS) (Agilent 7890A-GC with Agilent 5975C inert XL MSD) equipped with the VF-5ms column (0.25 mm ×30 m, film thickness 0.10 μm) with the electron ionization (EI) method (70eV). The oven temperature was programmed as follows: maintained at 40 °C for 2 min, raised up to 120 °C at 30 °C min^{-1}, then to 320 °C at 6 °C min^{-1}, and maintained at 320 °C for 20 min. Helium was used as the carrier gas with a constant flow are of 1 mL min^{-1}.

For the N-1 and N-2 fractions, no peaks were found. For the N-3 fraction, peaks around 12–13 min appeared both in the in-house Pheo *a* standard and the samples, suggesting that these are ionized fractions of Pheo *a* compound. Exogeneous compounds that were ionized by EI were not found except for pentacyclic triterpenoid compounds (simiarenol, β-amyrin, and their derivatives) eluting around 31–32 min, which were identified by commercial standard materials (simiarenol: HY-N1308 and β-amyrin: HY-N2922,

MedChemExpress, USA) (Figures S8 and S9) and by mass fragment patterns available in the literature (Elgamal et al., 1969; Galeron et al., 2016; Shiojima et al., 1992). (Figures S10–S17). The integrated peak areas of the impurities at the total ion chromatogram (TIC) were 8,992,239 and 14,639,503 for 1952 CE (Figures S10–S13) and 1968 CE (Figures S14–S17) samples, respectively.

To assess the carbon amount of simiarenol and β-amyrin (both $C_{30}H_{50}O$, 84% carbon) contained in the 1952 and 1968 Pheo *a* samples, their standard materials of 90 μg and 100 μg, respectively, were weighed using a microbalance (MC5, Sartorius, Germany). These were then dissolved into 2,000 μL of dichloromethane to make their final carbon concentrations of 38 ngC μL^{-1} and 43 ngC μL^{-1}, respectively, and were injected (1 μL) to GC/MS. The peak areas at TIC were 104,533,222 and 142,408,002, which were then used to conversion coefficients for TIC peak area per ngC as 2,753,482 and 3,376,019 for simiarenol and β-amyrin, respectively. Since simiarenol and β-amyrin were the major impurities contained in the 1952 and 1968 Pheo *a* samples, respectively, the conversion coefficients were then applied to their respective TIC peak areas to derive 0.33 μgC and 0.43 μgC. These amounts divided by their respective start amounts (2.5 μgC and 3.8 μgC) yield the percentages of simiarenol and β-amyrin as 13% and 11% for the 1952 and 1968 Pheo *a* samples, respectively.

Finally, the percentages of simiarenol and β-amyrin based on the GC/MS analysis were compared with the impurity carbon percentages estimated by C/N and Equation (4) (13% and 16% for the 1952 and 1968 Pheo *a* samples, respectively). The differences between the two estimates (0.2% and 4.4% for the 1952 and 1968 Pheo *a* samples, respectively) were smaller than our purity criterion (< 4.5%, 1σ) based on the C/N analytical error. Therefore, there is no evidence that the impurity in the purified Pheo *a* samples has carbon other than

simiarenol and β-amyrin. The details of comparison between triterpenoid carbon and impurity carbon are summarized in Table S1.

S2. Procedural Blank Analysis

We estimated the size of excess carbon associated with the entire experimental and analytical procedure (hereafter procedural blank, PB) (Fig. 2). The carbon mass (μgC) and $\Delta^{14}C$ (‰) of PB (M_{PB} and $\Delta^{14}C_{PB}$, respectively) have three components as follows.

$$M_{PB} = M_A + M_B + M_C, \quad \text{(S1)}$$

$$\Delta^{14}C_{PB} = \frac{M_A \times \Delta^{14}C_A + (M_B + M_C) \times \Delta^{14}C_{B+C}}{M_A + M_B + M_C}, \quad \text{(S2)}$$

where M_A, M_B, M_C, $\Delta^{14}C_A$, and $\Delta^{14}C_{B+C}$ are the carbon mass (μgC) and $\Delta^{14}C$ (‰) of (A) Wet chemistry blank, (B) EA/AMS capsule blank, and (C) EA/AMS machine blank, respectively.

M_A and M_B were estimated as 0.04 ± 0.06 μgC and 0.08 ± 0.01 μgC, respectively, using nano EA/IRMS. In brief, 200 μL of trichloromethane (TCM) was added to the vial that passed through (A) wet chemistry procedure using a precleaned glass syringe, 20 μL of which was transferred into a pre-cleaned (washed with DCM three times) tin capsule (3 mm diameter, 6 mm height, and 25 μL volume, P/N 84.9906.26, Lüdi Swiss, Switzerland) using a pre-cleaned glass syringe on a hot plate set at 80 ºC. Once dried, the tin capsule was introduced to the autosampler of nano EA/IRMS. Using the regression line between the nano EA/IRMS peak areas and carbon amounts of known working standards (L-tyrosine: BG-T, Tayasu et al., 2011), the (A) Wet chemistry blank M_A and (B) EA/AMS capsule blank M_B values were quantified for the above dried capsules and blank tin capsules, respectively (Figure S21). Four repeated measurements were performed. For calculation details, see Supplemental_Data.xlsx.

The sum of M_B and M_C was estimated as 0.28 ± 0.08 μgC using MICADAS (Haghipour et al., 2019). $\Delta^{14}C_{B+C}$ was determined as –303 ± 24‰ by analyzing five blank tin

capsules to achieve measurable carbon amounts using MICADAS (ETH analysis code 116866.2.1, $F^{14}C = 0.7034 \pm 0.0239$). The $\Delta^{14}C_A$ value is the only unknown in Equation S2, which might be derived from column bleed or organic solvents that had been potentially made from fossil-fuel products being depleted in ^{14}C. The $\Delta^{14}C_{Chl}$ value determined by MICADAS is represented using carbon mass (μgC) and $\Delta^{14}C$ of Chl *a*, impurity, and PB as follows.

$$\Delta^{14}C_{Chl} = \frac{(M_{Chl}+M_{Impurity})\times\Delta^{14}C_{Chl,corrected}+M_{PB}\times\Delta^{14}C_{PB}}{M_{Chl}+M_{Impurity}+M_{PB}}. \quad \text{(S3)}$$

Equation S3 is rewritten as follows.

$$\Delta^{14}C_{Chl,corrected} = \frac{(M_{Chl}+M_{Impurity}+M_{PB})\times\Delta^{14}C_{Chl}-M_{PB}\times\Delta^{14}C_{PB}}{M_{Chl}+M_{Impurity}}. \quad \text{(S4)}$$

We examined the effect of $\Delta^{14}C_A$ (i.e., wet chemistry blank) on the corrected $\Delta^{14}C_{Chl}$ values of the four Chl *a* data that satisfied the purity criterion and are used for modelling (1973, 1982, 1995, and 2007 CE, Table 1) (Figure S22). Even in the most extreme case where the $\Delta^{14}C_A$ was –1,000‰, the corrected $\Delta^{14}C_{Chl}$ values were within the MICADAS analytical error (± 8‰, 1σ) of their respective uncorrected $\Delta^{14}C_{Chl}$ values. Therefore, we concluded that the procedural blank does not analytically influence the observed $\Delta^{14}C_{Chl}$ values.

An aliquot (20 μL) of (A) Wet chemistry blank (dissolved in 200 μL TCM) was split into a pre-cleaned glass vial and dried. BSTFA was added to the vial and heated at 40 °C to derivatize the TMS ester. After drying with argon gas, the TMS ester was redissolved in 100 μL of dichloromethane and was injected (1 μL) to GC/MS with the same method being mentioned in the purity assessment. We found trace amounts of benzoic acid TMS derivative (Figure S23) and diethyl phthalate (Figure S24), which may have been derived from somewhere in the experimental procedure.

S3. Sensitivity Analysis

Our assumption of the leaf turnover time (T_Q, set as 1.5 years) refers to a previous study working on $\Delta^{14}C$ analysis of the *Quercus* oak (Ichie et al., 2013). We carried out a sensitivity analysis by tweaking the T_Q values from 0.5 to 5.0 years, and no substantial change was observed (Figure S25), suggesting that the model estimates are insensitive to the T_Q values at this range. It should be noted that the leaf turnover time ≥ 5.0 years is unlikely because such an endmember cannot explain the 1965 and 1966 data (Figure S2).

Supplemental References

Elgamal, M. H. A., Fayez, M. B. E., & Kemp, T. R. (1969). The mass spectra of some triterpenoid dehydration products. *Organic Mass Spectrometry*, *2*(2), 175–194. https://doi.org/10.1002/oms.1210020204

Galeron, M. A., Vaultier, F., & Rontani, J. F. (2016). Oxidation products of α- And β-amyrins: Potential tracers of abiotic degradation of vascular-plant organic matter in aquatic environments. *Environmental Chemistry*, *13*(4), 732–744. https://doi.org/10.1071/EN15237

Haghipour, N., Ausin, B., Usman, M. O., Ishikawa, N., Wacker, L., Welte, C., Ueda, K., & Eglinton, T. I. (2019). Compound-Specific Radiocarbon Analysis by Elemental Analyzer–Accelerator Mass Spectrometry: Precision and Limitations. *Analytical Chemistry*, *91*(3), 2042–2049. https://doi.org/10.1021/acs.analchem.8b04491

Ichie, T., Igarashi, S., Yoshida, S., Kenzo, T., Masaki, T., & Tayasu, I. (2013). Are stored carbohydrates necessary for seed production in temperate deciduous trees? *Journal of Ecology*, *101*(2), 525–531. https://doi.org/10.1111/1365-2745.12038

Ischebeck, T., Zbierzak, A. M., Kanwischer, M., & Dörmann, P. (2006). A salvage pathway for phytol metabolism in Arabidopsis. *Journal of Biological Chemistry*, *281*(5), 2470–2477. https://doi.org/10.1074/jbc.M509222200

Shiojima, K., Arai, Y., Masuda, K., Takase, Y., Ageta, T., & Ageta, H. (1992). Mass Spectra of Pentacyclic Triterpenoids. *Chemical and Pharmaceutical Bulletin*, *40*(7), 1683–1690. https://doi.org/10.1248/cpb.40.1683

Tayasu, I., Hirasawa, R., Ogawa, N. O., Ohkouchi, N., & Yamada, K. (2011). New organic reference materials for carbon- and nitrogen-stable isotope ratio measurements provided by Center for Ecological Research, Kyoto University, and Institute of Biogeosciences, Japan Agency for Marine-Earth Science and Technology. *Limnology*, *12*(3), 261–266. https://doi.org/10.1007/s10201-011-0345-5

Vavilin, D., & Vermaas, W. (2007). Continuous chlorophyll degradation accompanied by chlorophyllide and phytol reutilization for chlorophyll synthesis in Synechocystis sp. PCC 6803. *Biochimica et Biophysica Acta - Bioenergetics*, *1767*(7), 920–929. https://doi.org/10.1016/j.bbabio.2007.03.010

Tabe S1. Comparison between triterpenoid carbon and impurity carbon

Triterpenoid Standards	**Simiarenol**	**β-amyrin**	Notes
Formula	$C_{30}H_{50}O$	$C_{30}H_{50}O$	MW: 426.72
%C	84%	84%	(A)
Weighed (μg)	90	100	(B)
Dichloromethane total volume (μL)	2000	2000	(C)
Concentration (ngC μL^{-1})	38	42	(D) = (A)x(B)/(C)x1000
GC/MS Injection volume (μL)	1	1	(E)
TIC area on GC/MS	104533222	142408002	(F)
TIC area ngC^{-1}	2753482	3376019	(G) = (F)/(D)x(E)
Purified Pheo *a* Sample	**1952 CE**	**1968 CE**	Notes
μgC analyzed	2.5	3.8	(H)
Dichloromethane total volume (μL)	100	100	(I)
Concentration (ngC μL^{-1})	25	38	(J) = (H)/(I)x1000
GC/MS Injection volume (μL)	1	1	(K)
TIC area on GC/MS	8992239	14639503	(L)
μgC impurity	0.33	0.43	(M) = (L)/(G)x(I)/(K)x1000
%Triterpenoid Carbon	**13%**	**11%**	**(N) = (H)/(M)**
C/N expected for Pheo *a*	11.8	11.8	(O) = 55x12.01/4/14.0067
C/N observed on EA/IRMS	13.6	14.0	(P)
%Impurity Carbon	**13%**	**16%**	**(Q) = 1 – (O)/(P), See Equation (4)**
Comparison between triterpenoids and impurities	**0.2%**	**4.4%**	**(R) = (Q) – (N)**

TIC: Total ion chromatogram

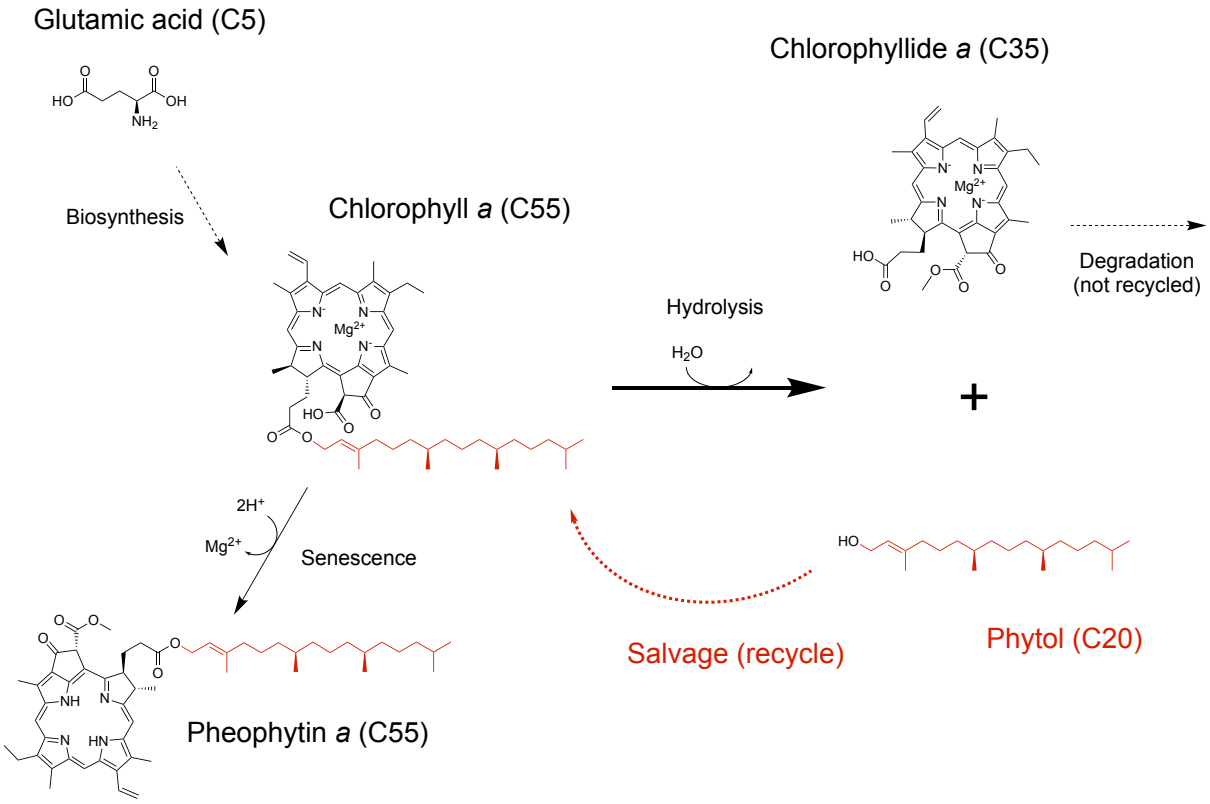

Figure S1. Summary of key reactions in chlorophyll *a* anabolism and catabolism (Ischebeck et al., 2006; Vavilin & Vermaas, 2007) highlighted in the present study.

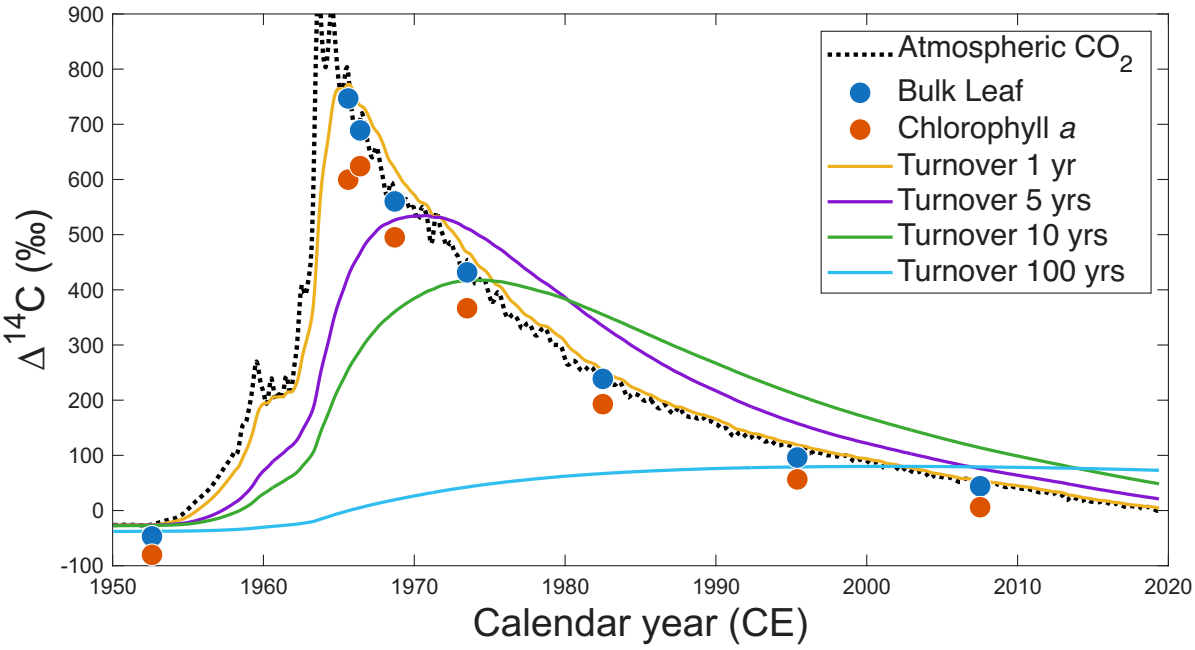

Figure S2. The difference in turnover times of the carbon source on the $\Delta^{14}C$ vs. calendar year biplot space.

Figure S3a. HPLC/DAD spectrums of Pheo *a* collected through separation using the C18 (1st) and PAH (2nd) columns in 1952 CE. Dashed lines indicate fraction collection window (16.5–20.5 min).

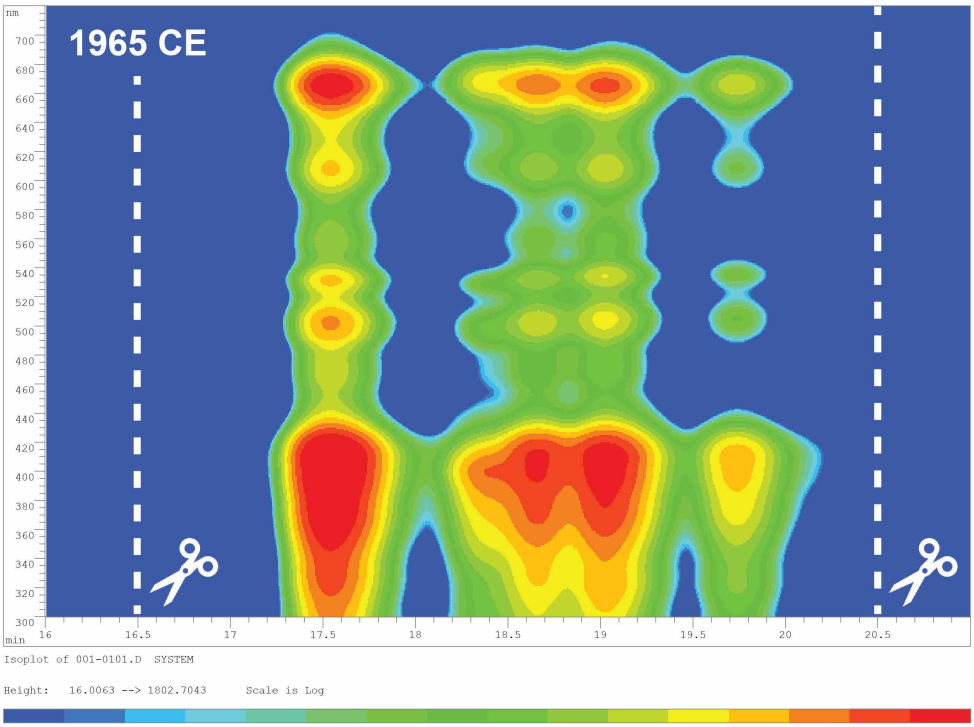

Figure S3b. HPLC/DAD spectrums of Pheo *a* collected through separation using the C18 (1st) and PAH (2nd) columns in 1965 CE. Dashed lines indicate fraction collection window (16.5–20.5 min).

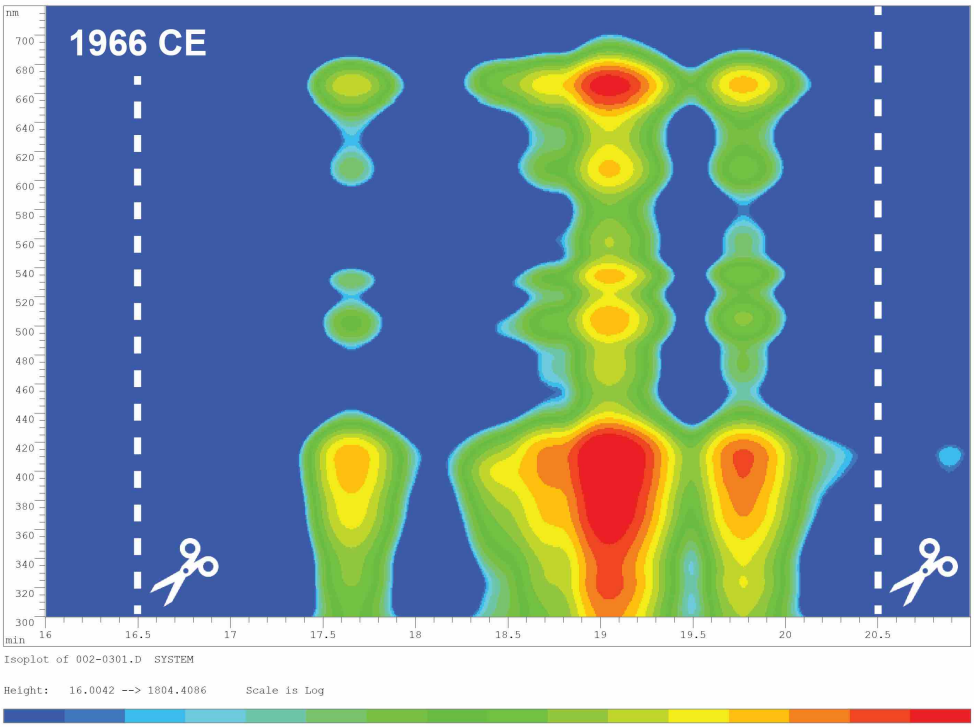

Figure S3c. HPLC/DAD spectrums of Pheo *a* collected through separation using the C18 (1st) and PAH (2nd) columns in 1966 CE. Dashed lines indicate fraction collection window (16.5–20.5 min).

Figure S3d. HPLC/DAD spectrums of Pheo *a* collected through separation using the C18 (1st) and PAH (2nd) columns in 1968 CE. Dashed lines indicate fraction collection window (16.5–20.5 min).

Figure S3e. HPLC/DAD spectrums of Pheo *a* collected through separation using the C18 (1st) and PAH (2nd) columns in 1973 CE. Dashed lines indicate fraction collection window (16.5–20.5 min).

Figure S3f. HPLC/DAD spectrums of Pheo *a* collected through separation using the C18 (1st) and PAH (2nd) columns in 1982 CE. Dashed lines indicate fraction collection window (16.5–20.5 min).

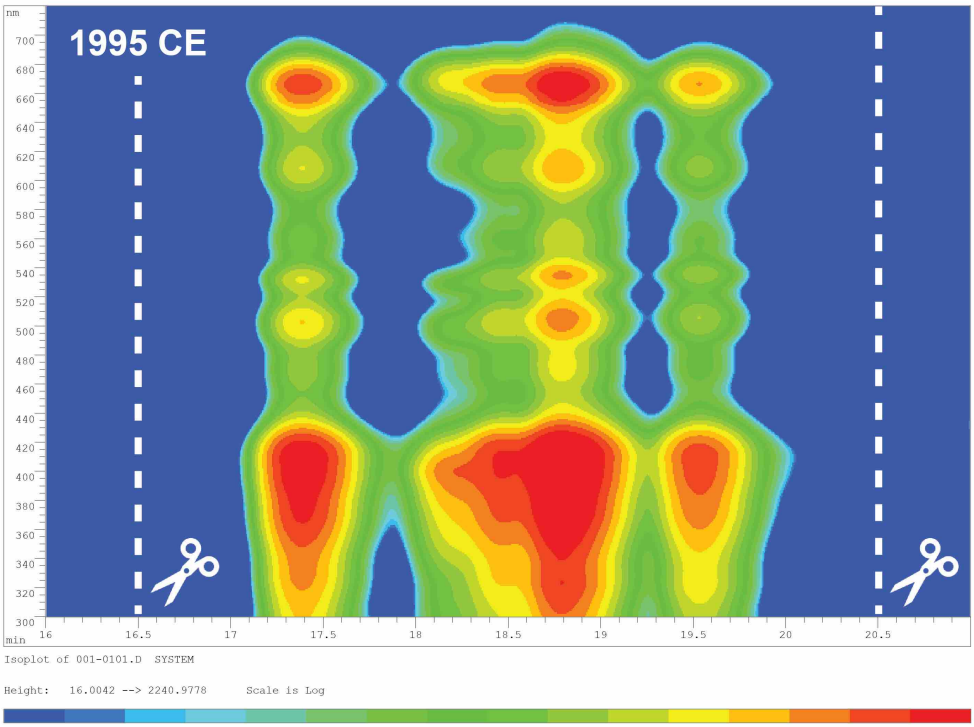

Figure S3g. HPLC/DAD spectrums of Pheo *a* collected through separation using the C18 (1st) and PAH (2nd) columns in 1995 CE. Dashed lines indicate fraction collection window (16.5–20.5 min).

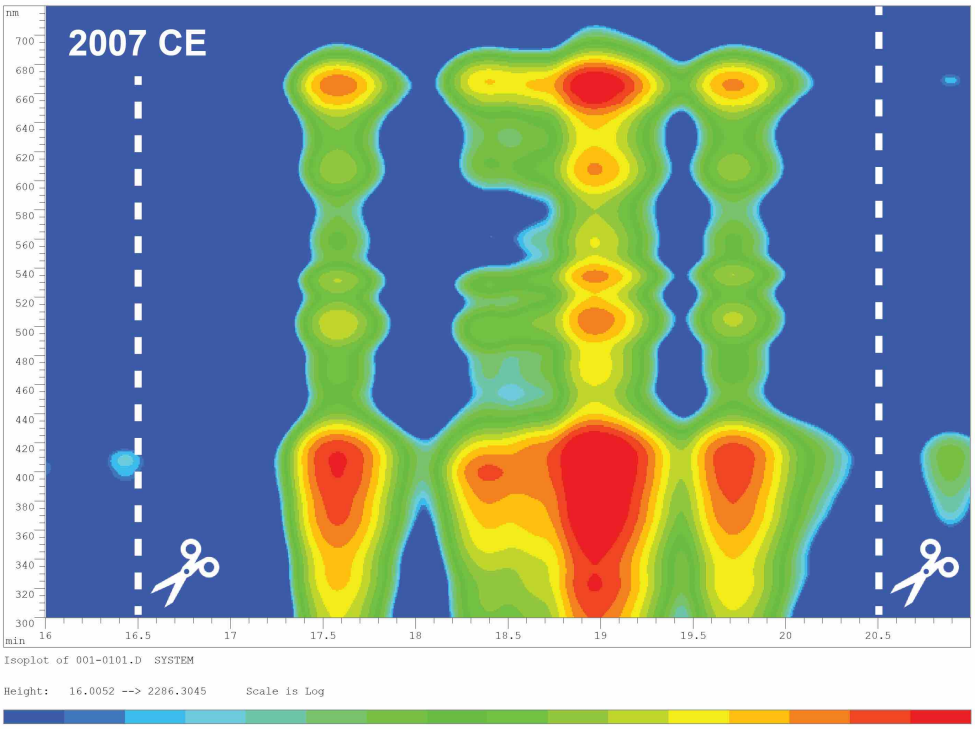

Figure S3h. HPLC/DAD spectrums of Pheo *a* collected through separation using the C18 (1st) and PAH (2nd) columns in 2007 CE. Dashed lines indicate fraction collection window (16.5–20.5 min).

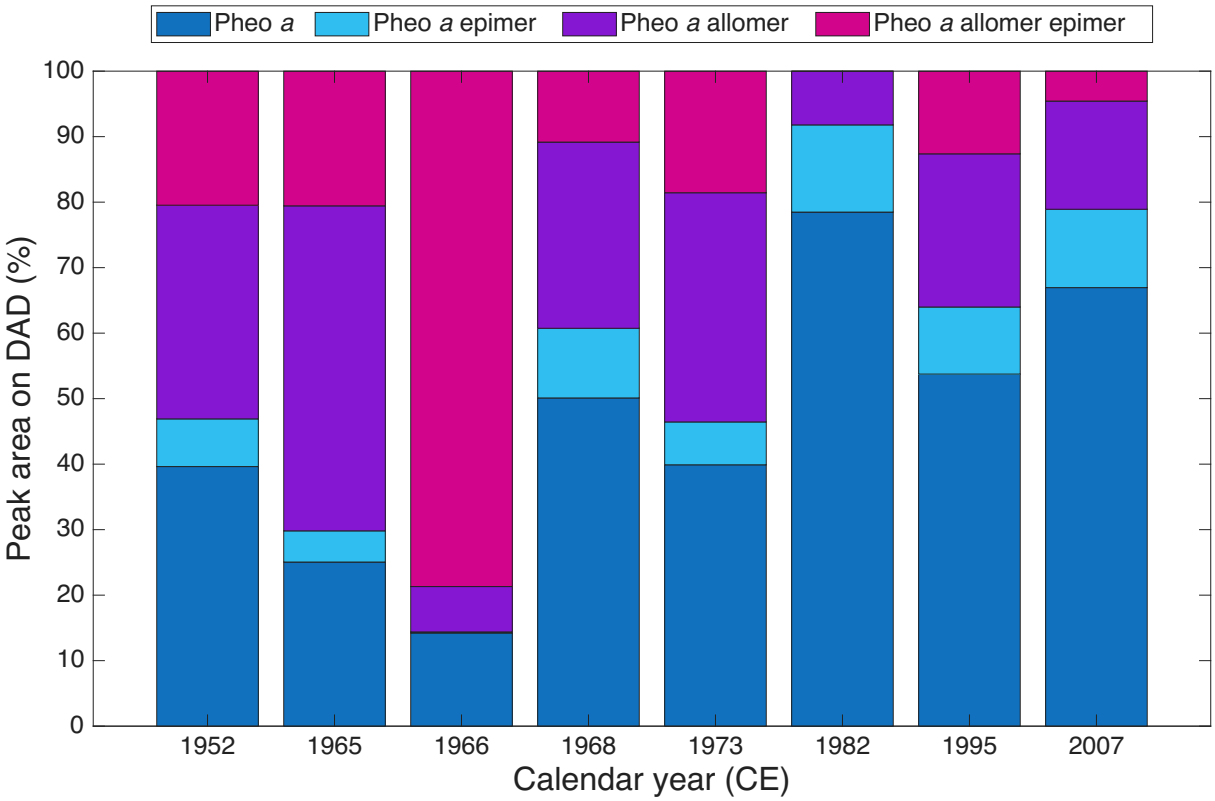

Figure S4. DAD peak area (660 nm) percentage of Pheo *a* allomer (16.5–17.8 min), Pheo *a* allomer epimer, Pheo *a* (17.8–19.2 min), and Pheo *a* epimer (19.2–20.5 min).

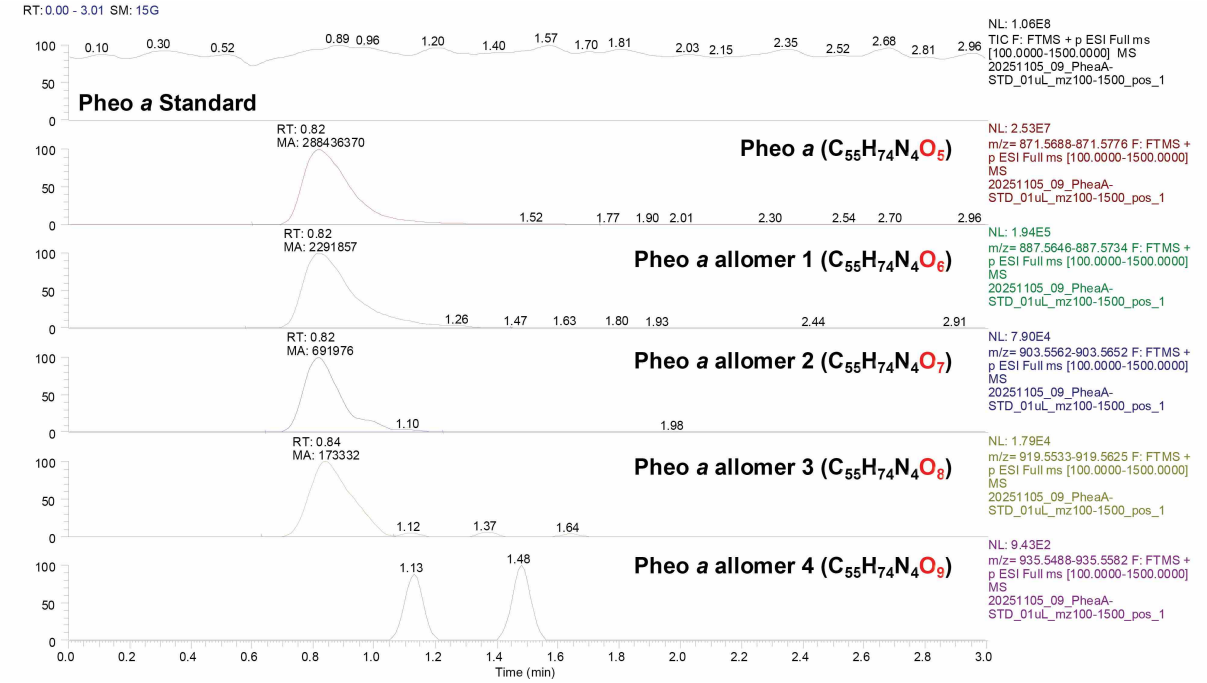

Figure S5a. Orbitrap MS chromatograms of Pheo *a* (*m/z* 871.6, $C_{55}H_{74}N_4O_5$) in an in-house standard.

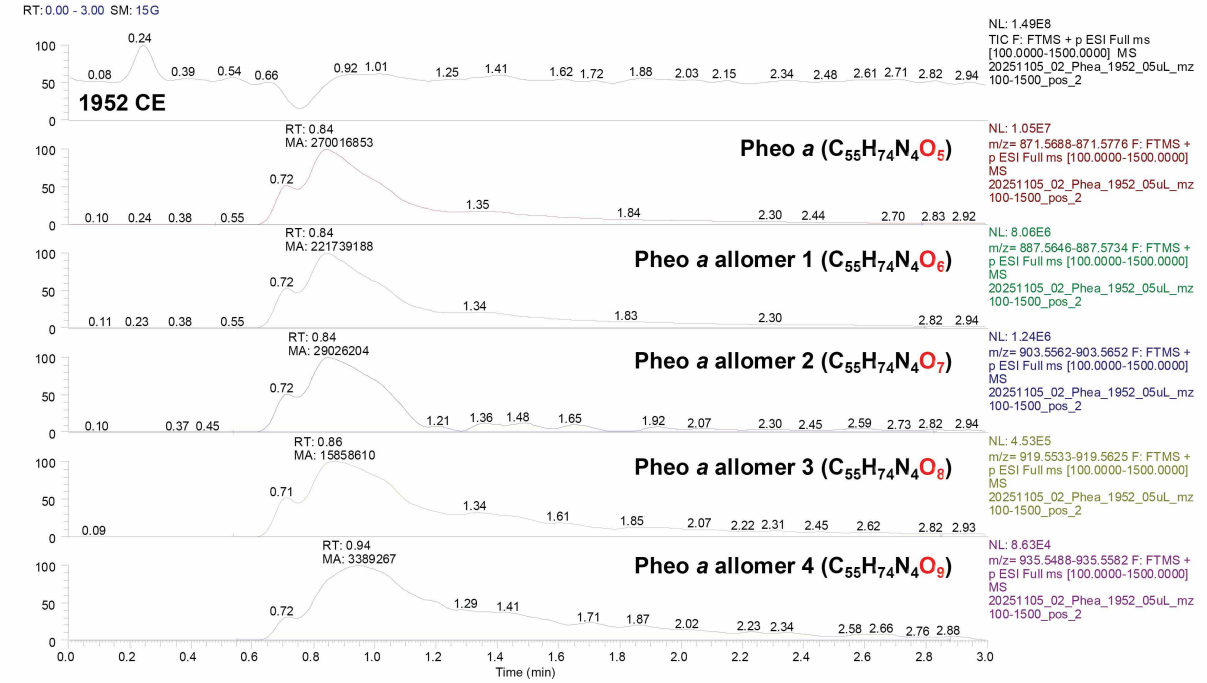

Figure S5b Orbitrap MS chromatograms of Pheo *a* (*m/z* 871.6, $C_{55}H_{74}N_4O_5$) in 1952 CE.

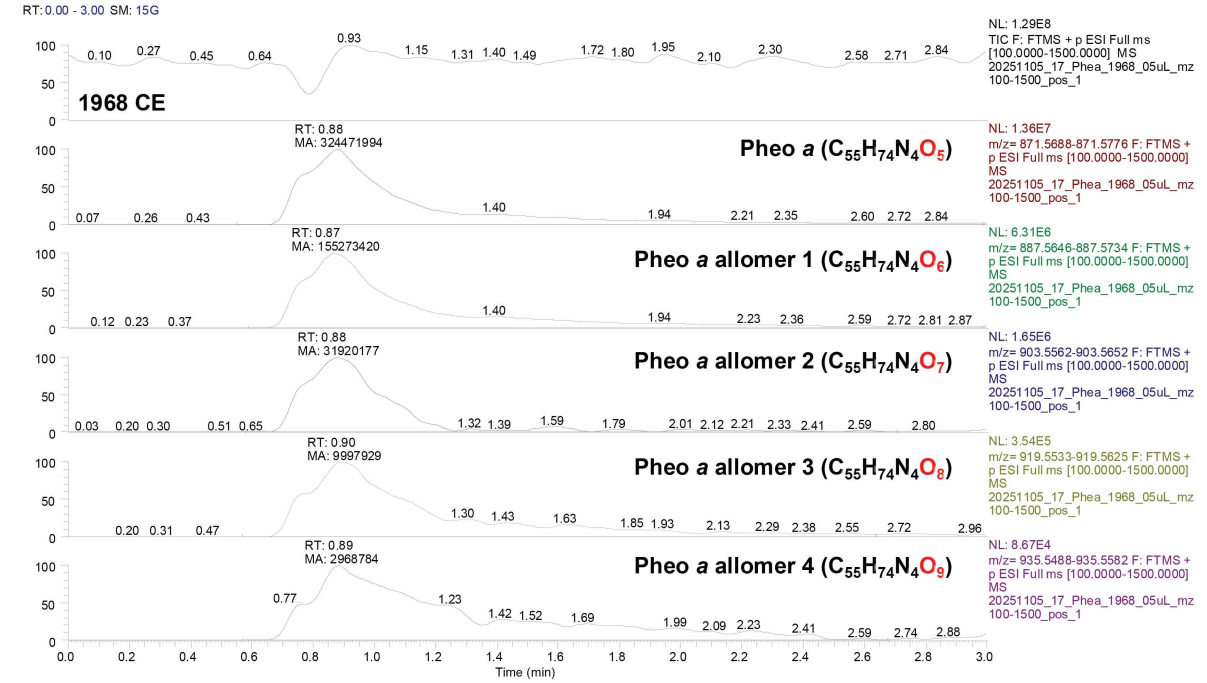

Figure S5c. Orbitrap MS chromatograms of Pheo *a* (*m/z* 871.6, $C_{55}H_{74}N_4O_5$) in 1968 CE.

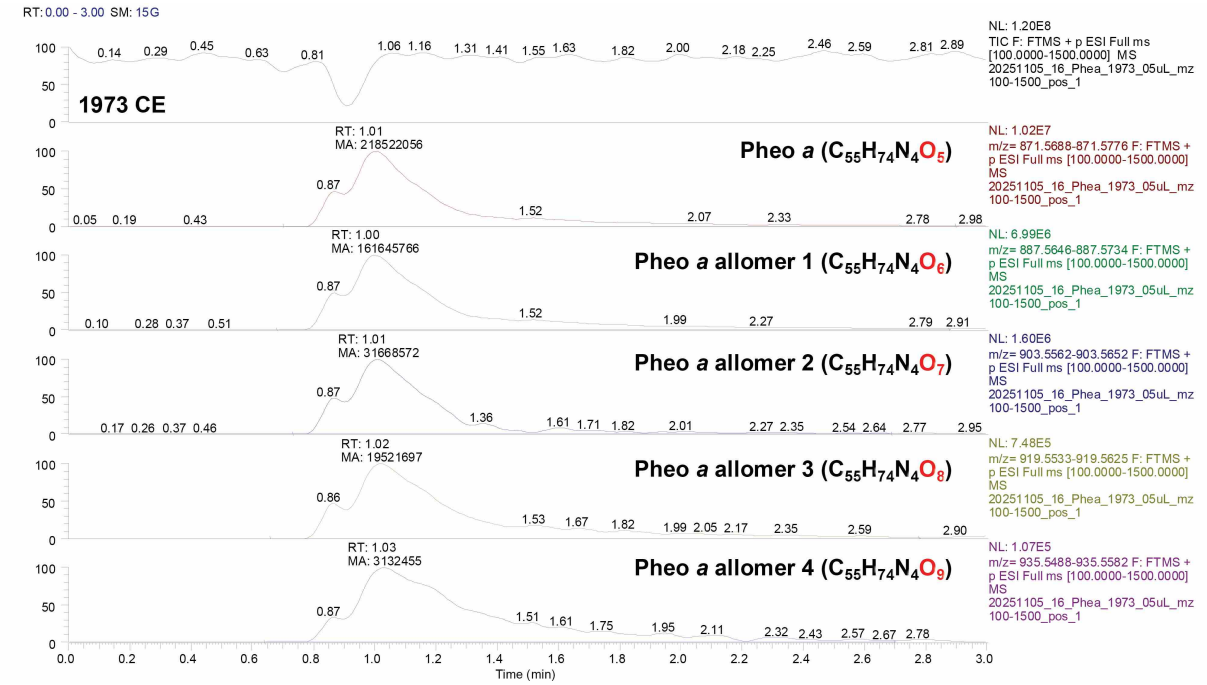

Figure S5d. Orbitrap MS chromatograms of Pheo *a* (*m/z* 871.6, $C_{55}H_{74}N_4O_5$) in 1973 CE.

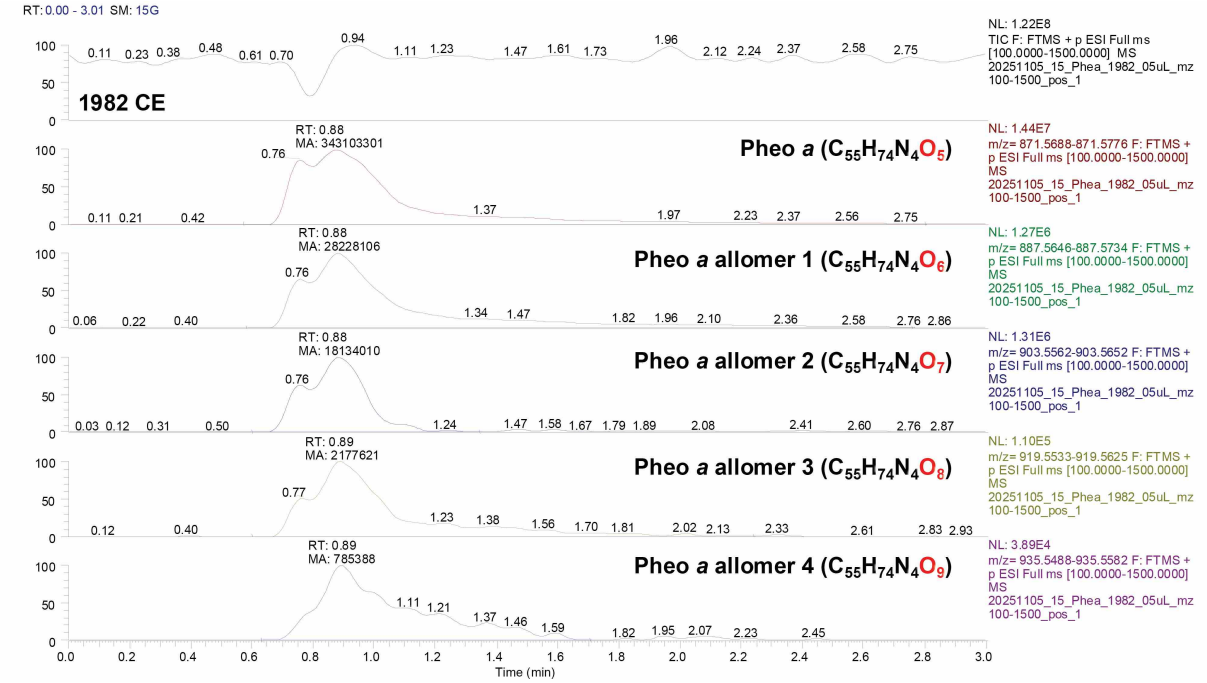

Figure S5e. Orbitrap MS chromatograms of Pheo *a* (*m/z* 871.6, $C_{55}H_{74}N_4O_5$) in 1982 CE.

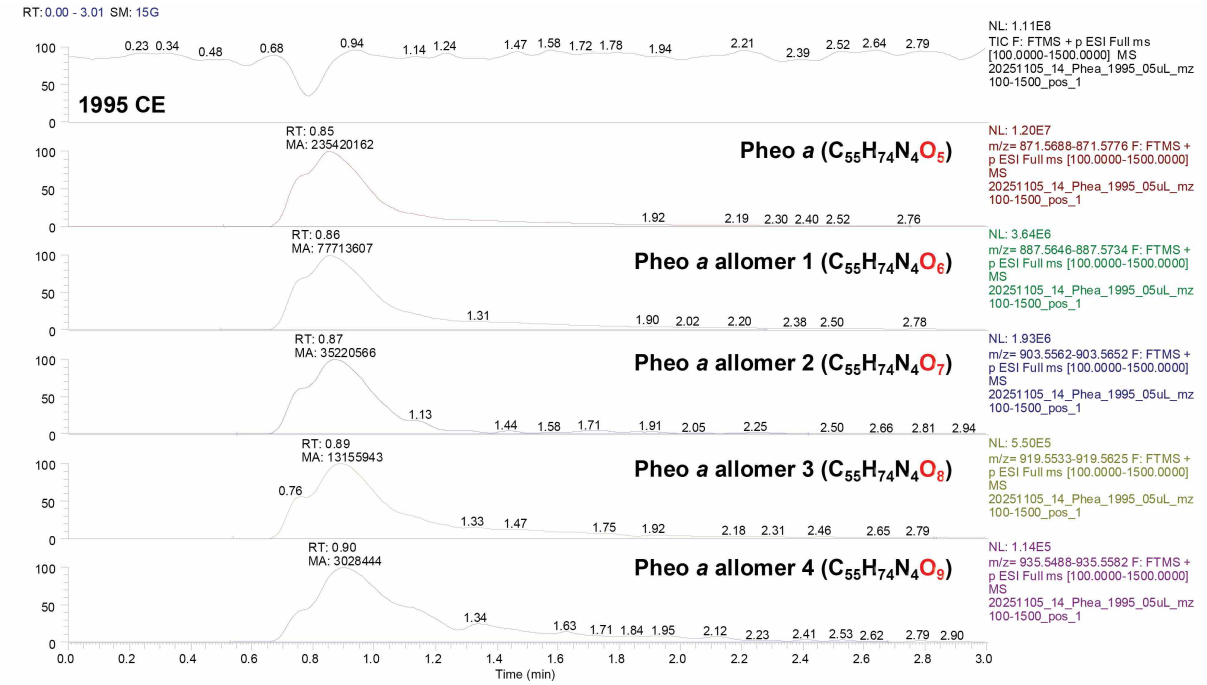

Figure S5f. Orbitrap MS chromatograms of Pheo *a* (*m/z* 871.6, $C_{55}H_{74}N_4O_5$) in 1995 CE.

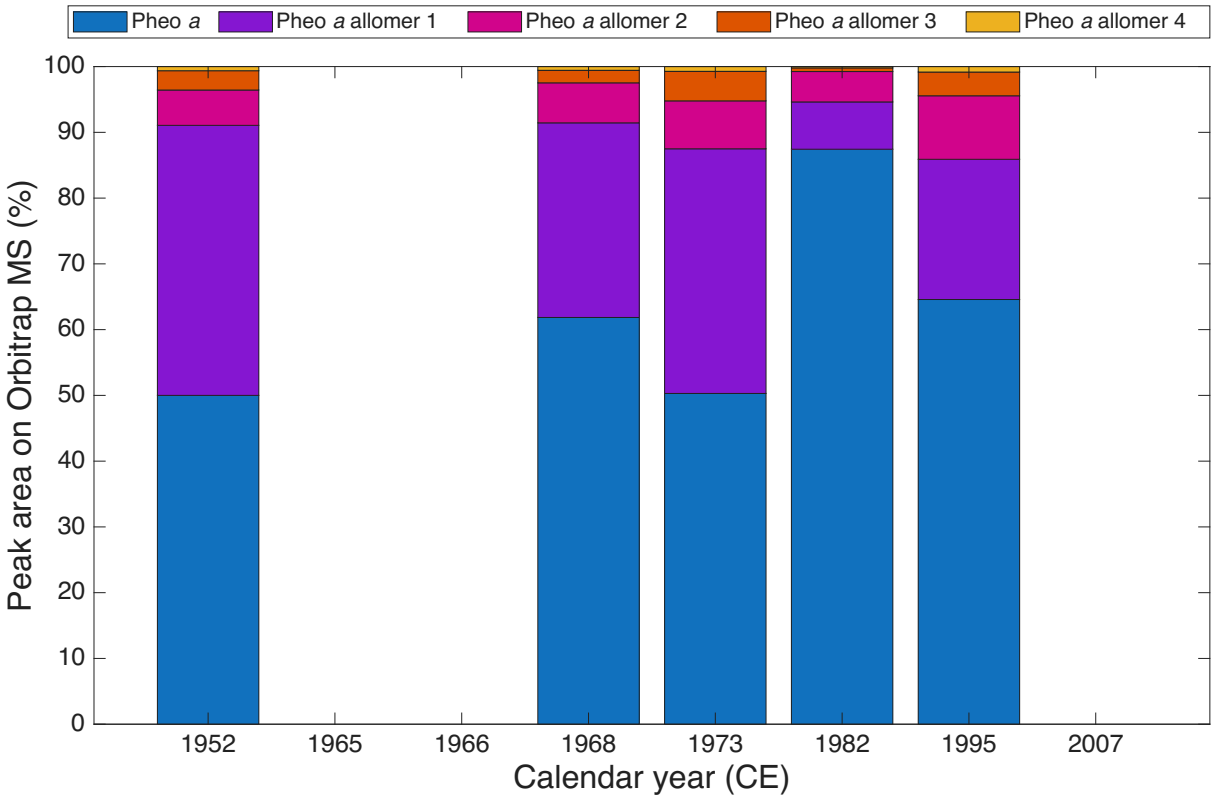

Figure S6. Orbitrap MS peak area percentage of Pheo *a* and its allomers.

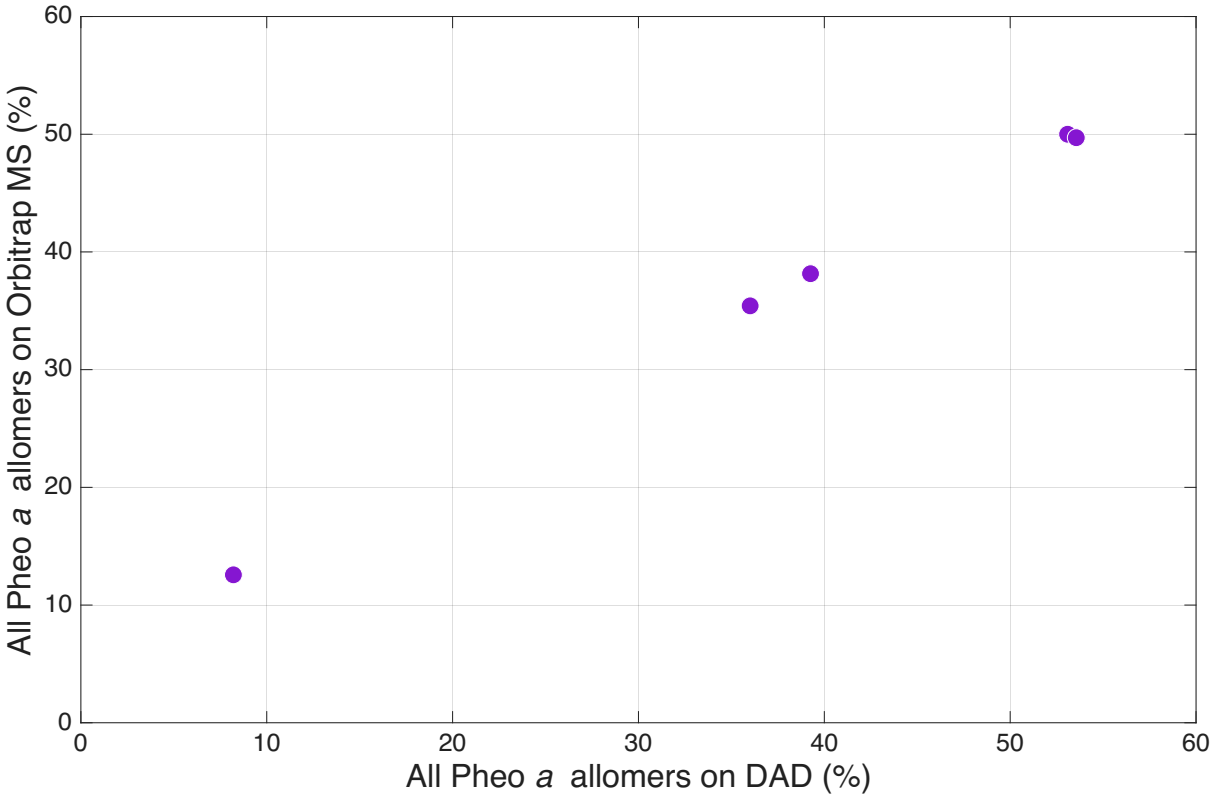

Figure S7. Relationship between DAD peak area (660 nm) percentage and Orbitrap MS peak area percentage of Pheo *a* and its allomers. The strong positive correlation corroborates that the compounds are Pheo *a* derivatives (allomers).

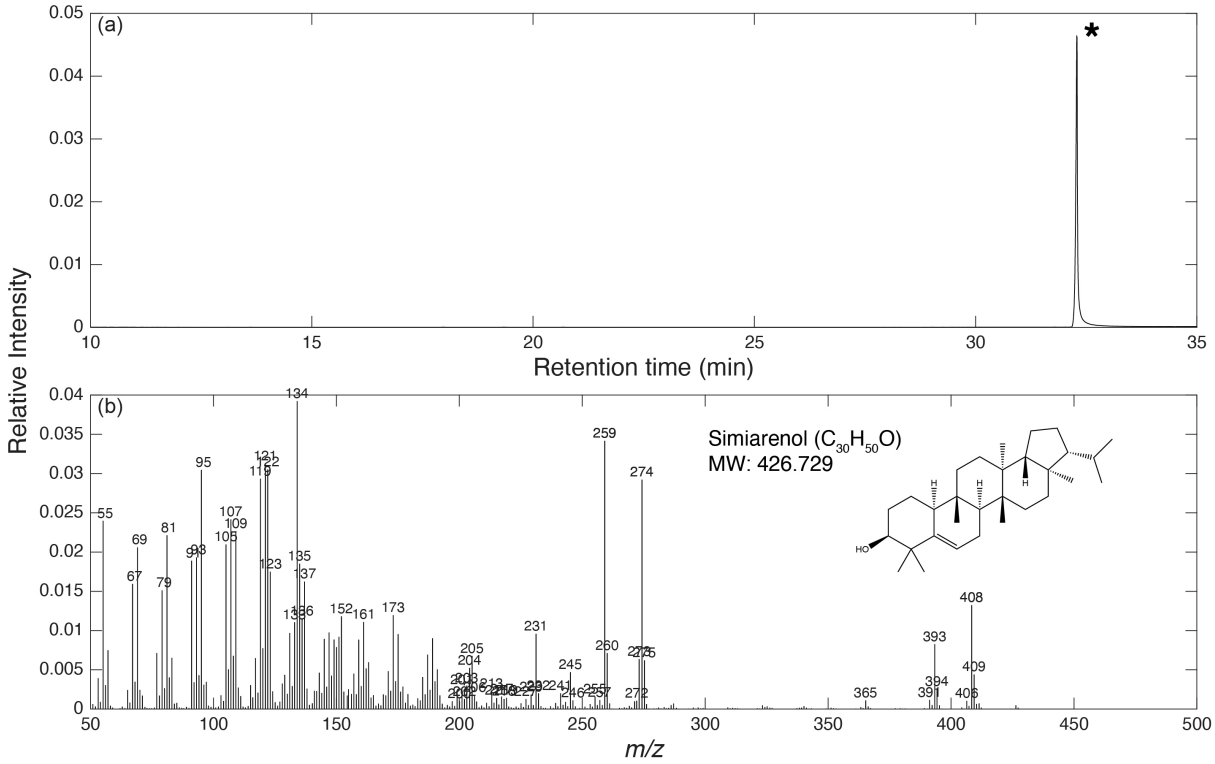

Figure S8. (a) Total ion chromatogram and (b) mass spectrum of the simiarenol standard. The asterisk denotes the peak for which the mass spectrum is obtained.

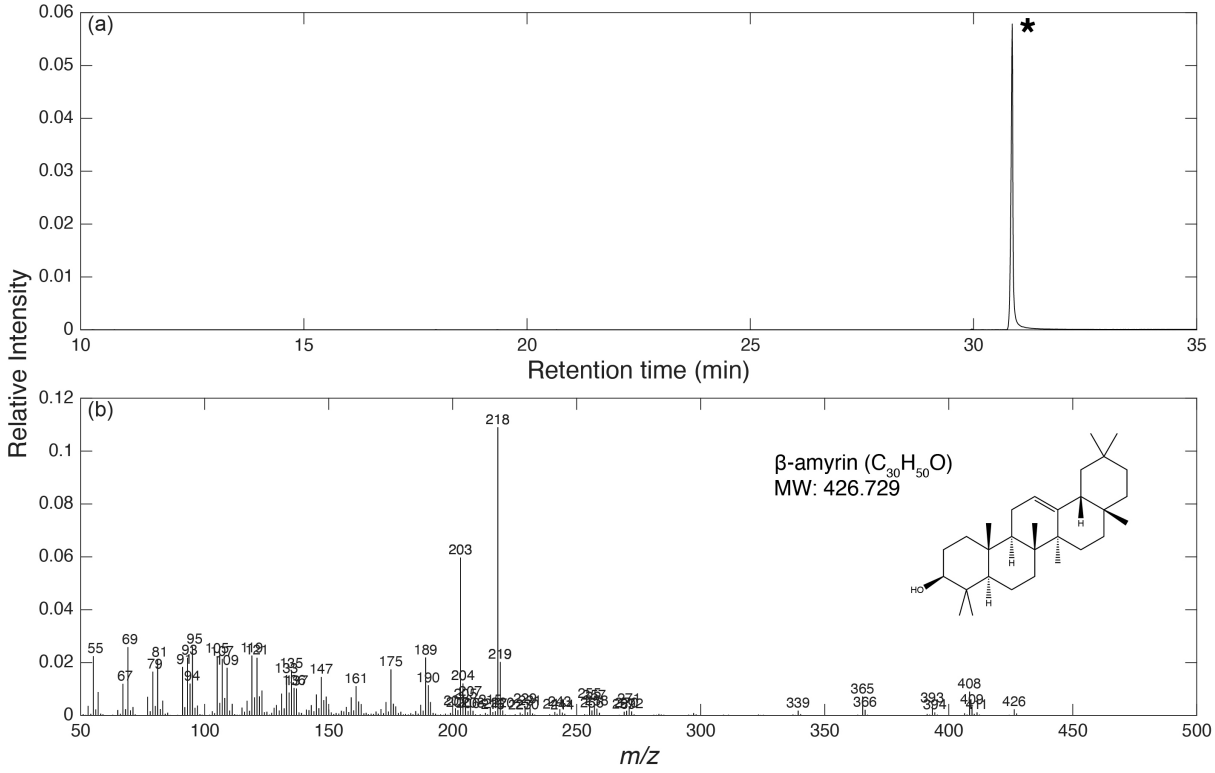

Figure S9. (a) Total ion chromatogram and (b) mass spectrum of the β-amyrin standard. The asterisk denotes the peak for which the mass spectrum is obtained.

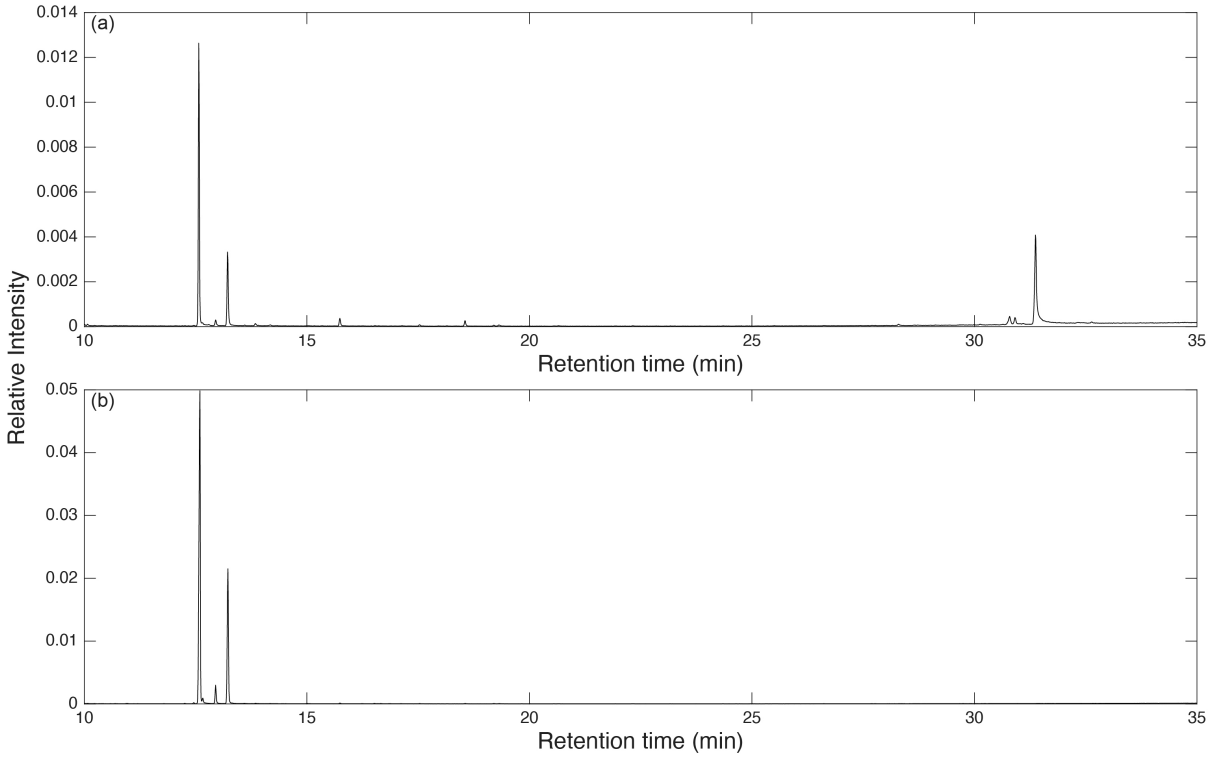

Figure S10. Total ion chromatogram of the N-3 fraction (a) in an in-house standard Pheo *a* and (b) in Pheo *a* extracted from the *Quercus pubescens* leaf collected in 1952 CE and purified for CSRA.

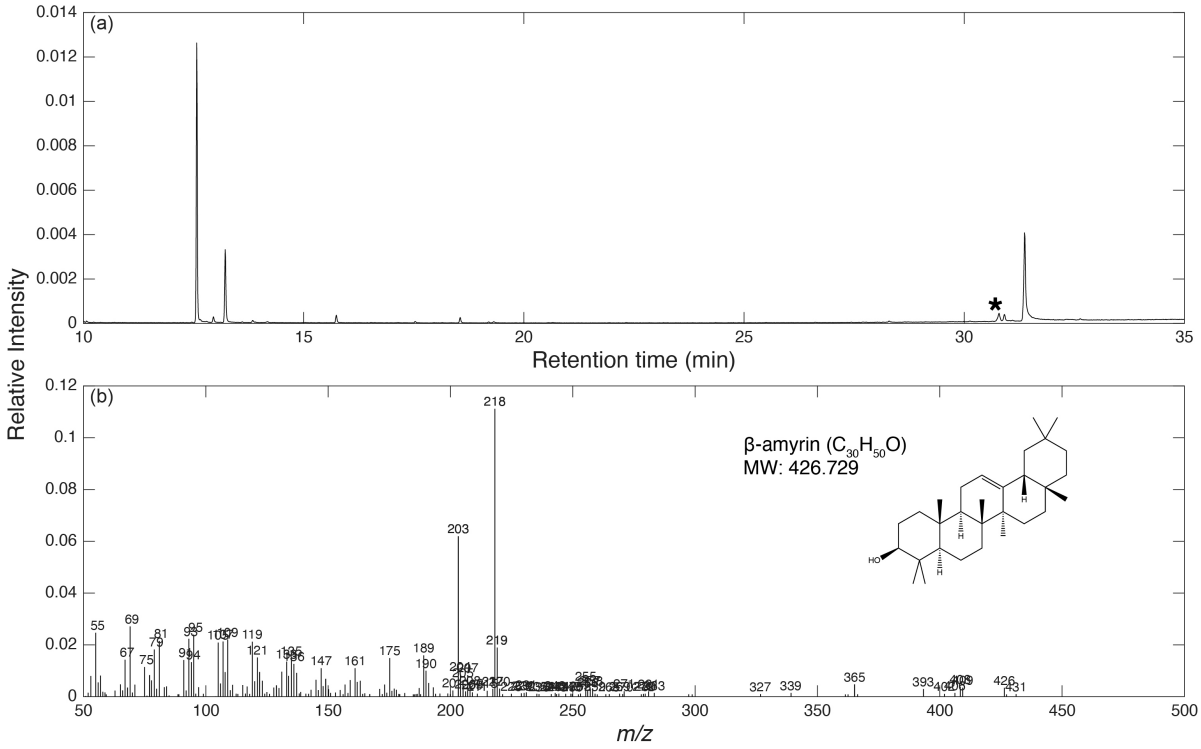

Figure S11. (a) Total ion chromatogram and (b) mass spectrum of the first unknown peak of the N-3 fraction in Pheo *a* in 1952 CE. The asterisk denotes the peak for which the mass spectrum is obtained.

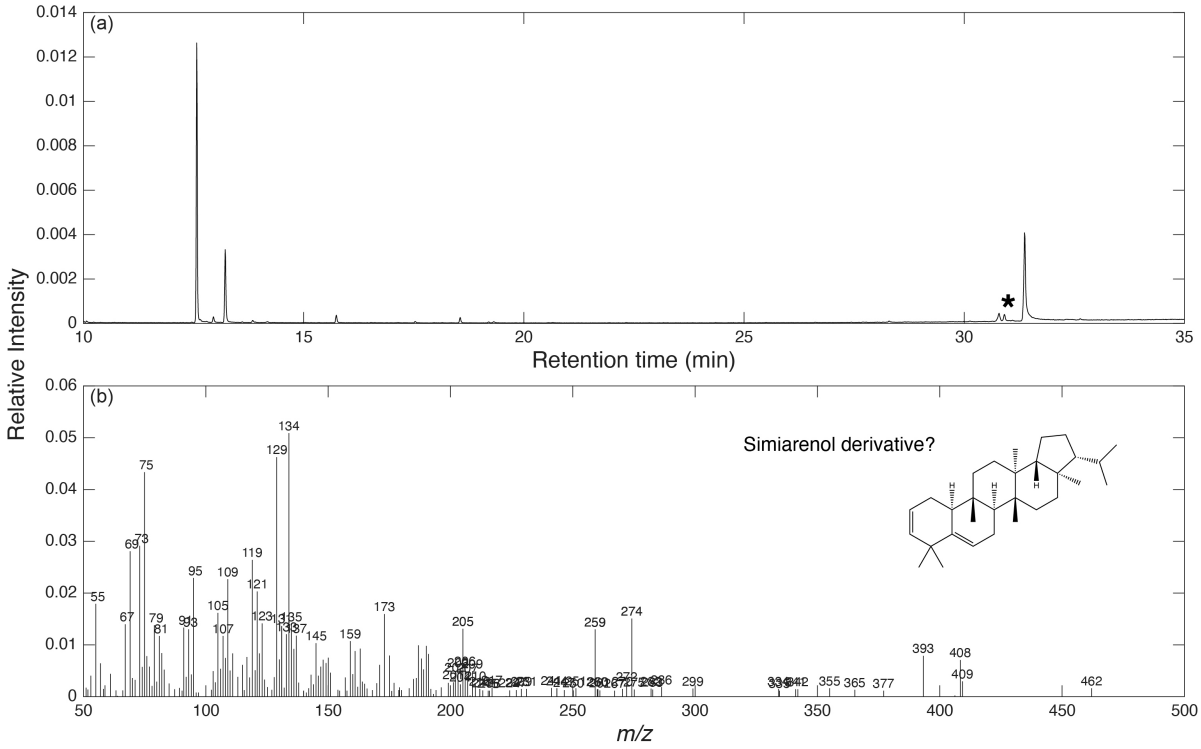

Figure S12. (a) Total ion chromatogram and (b) mass spectrum of the second unknown peak of the N-3 fraction in Pheo *a* in 1952 CE. The asterisk denotes the peak for which the mass spectrum is obtained.

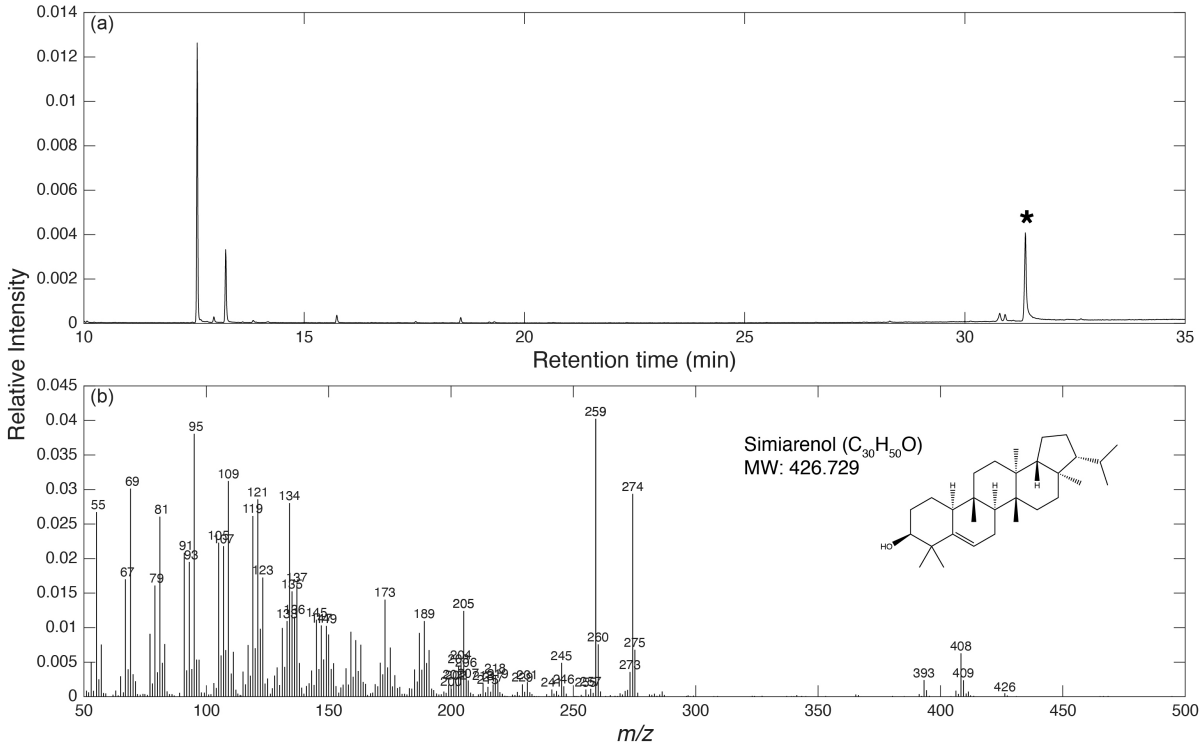

Figure S13. (a) Total ion chromatogram and (b) mass spectrum of the third unknown peak of the N-3 fraction in Pheo *a* in 1952 CE. The asterisk denotes the peak for which the mass spectrum is obtained.

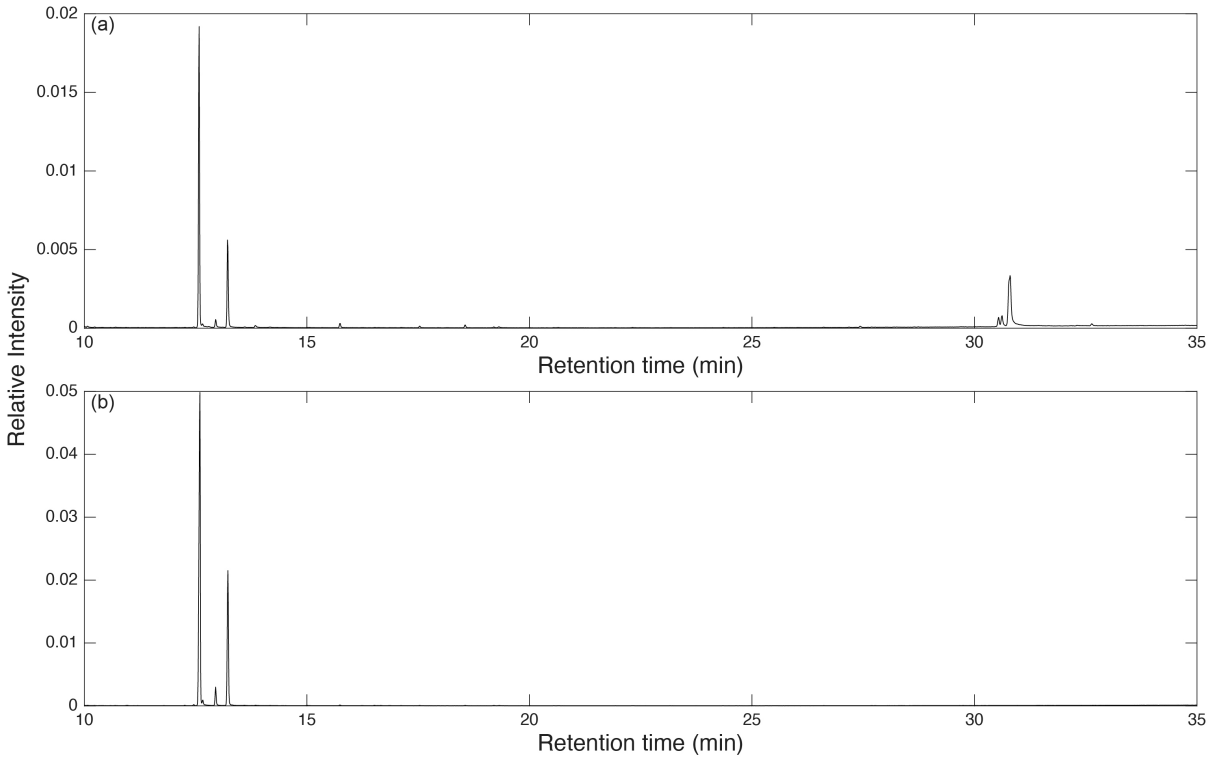

Figure S14. Total ion chromatogram of the N-3 fraction (a) in an in-house standard Pheo *a* and (b) in Pheo *a* extracted from the *Quercus pubescens* leaf collected in 1968 CE and purified for CSRA.

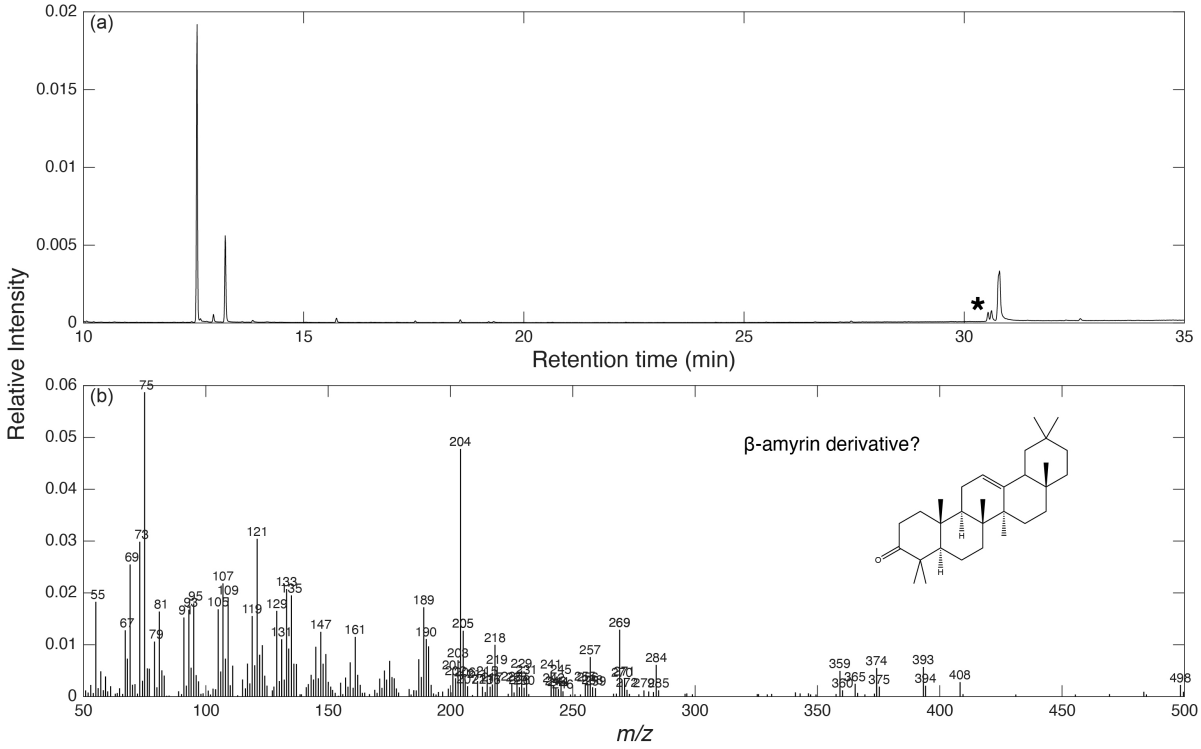

Figure S15. (a) Total ion chromatogram and (b) mass spectrum of the first unknown peak of the N-3 fraction in Pheo *a* in 1968 CE. The asterisk denotes the peak for which the mass spectrum is obtained.

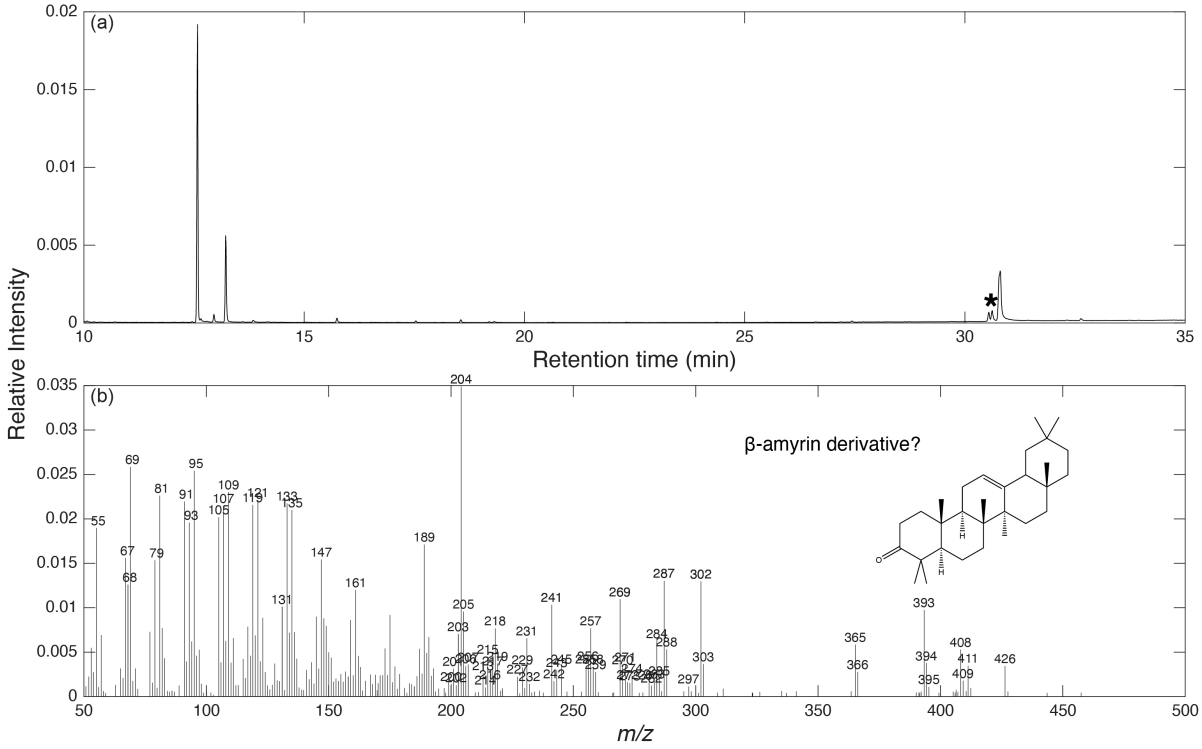

Figure S16. (a) Total ion chromatogram and (b) mass spectrum of the second unknown peak of the N-3 fraction in Pheo *a* in 1968 CE. The asterisk denotes the peak for which the mass spectrum is obtained.

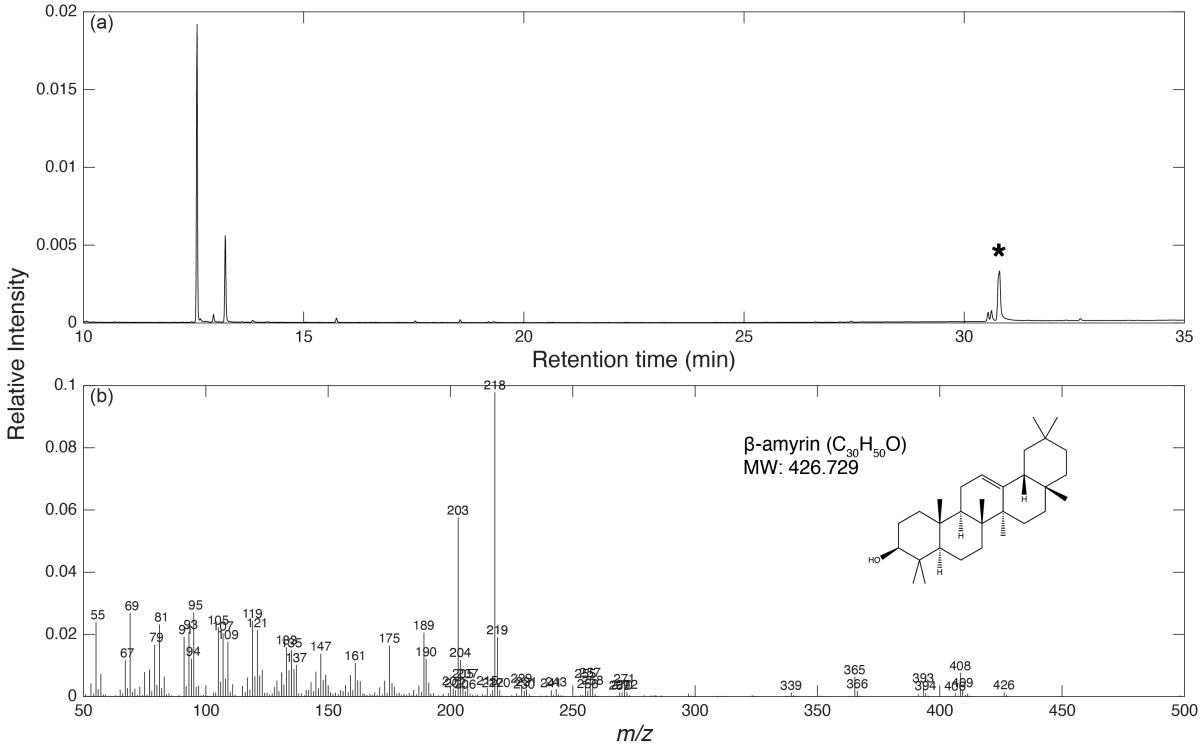

Figure S17. (a) Total ion chromatogram and (b) mass spectrum of the third unknown peak of the N-3 fraction in Pheo *a* in 1968 CE. The asterisk denotes the peak for which the mass spectrum is obtained.

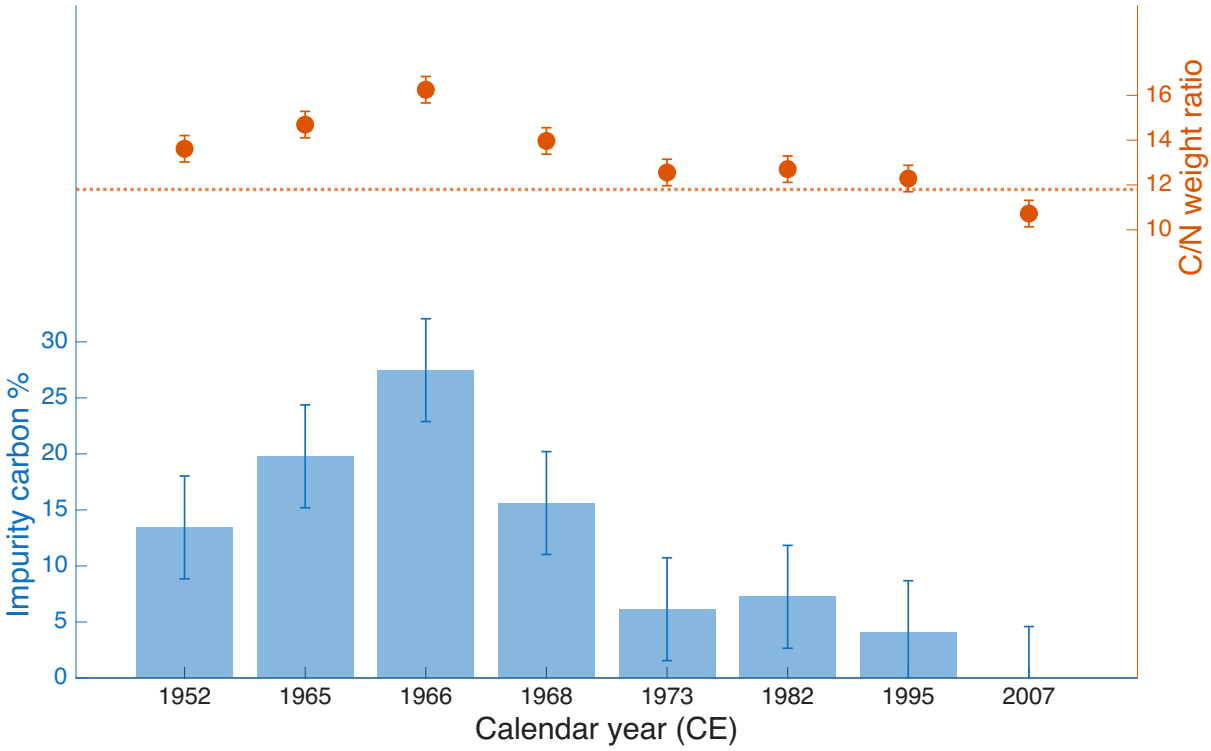

Figure S18. The observed C/N ratios (right axis in red) and blank carbon % (left axis in blue) for Chl *a* purified from *Quercus* leaf samples plotted against collection year CE. Error bars indicate 1σ uncertainties. The dashed red line indicates expected C/N ratios of Chl *a* (11.8). The four older samples collected in 1952, 1965, 1966, and 1968 CE showed significantly higher C/N and blank carbon % than 11.8 and 0, respectively, while the four newer samples collected in 1973, 1982, 1995, and 2007 CE did not.

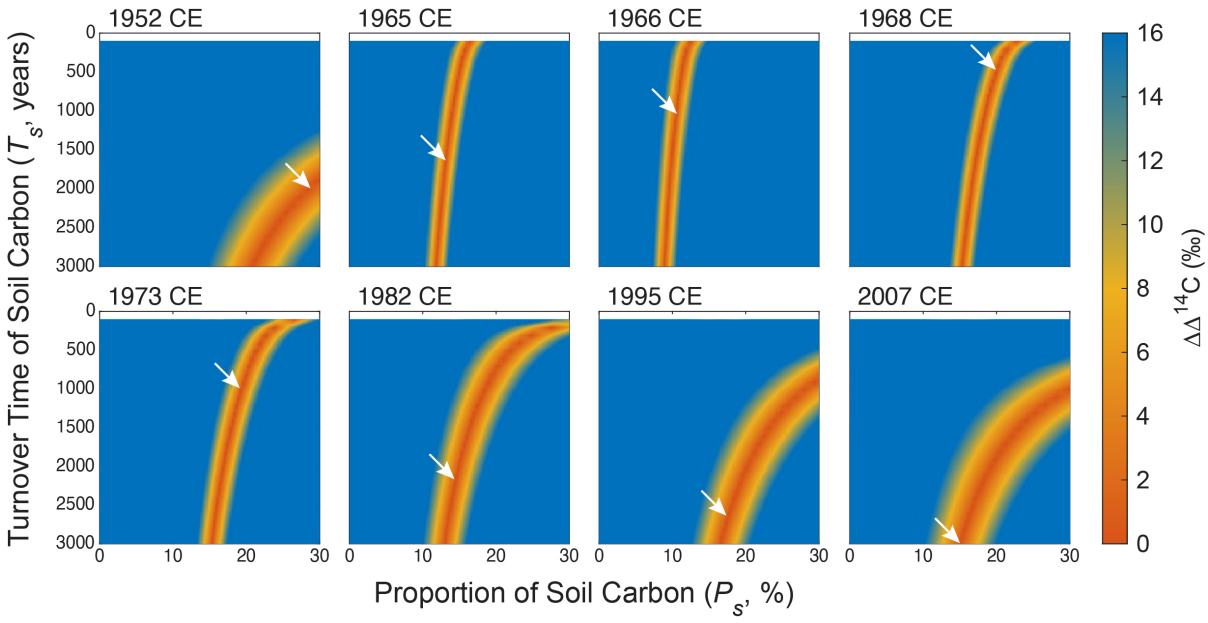

Figure S19. Heatmaps of the difference ($\Delta\Delta^{14}C$) between observed and modelled $\Delta^{14}C_{Chl}$ values on a biplot for soil turnover time (T_s, years) versus soil proportion (P_s, %) for each of the eight samples collected in different years. The $\Delta\Delta^{14}C$ value larger than the 2σ analytical error of CSRA (>16‰) was not considered in this plot. The white arrows denote the smallest $\Delta\Delta^{14}C$ values (i.e., the most plausible models).

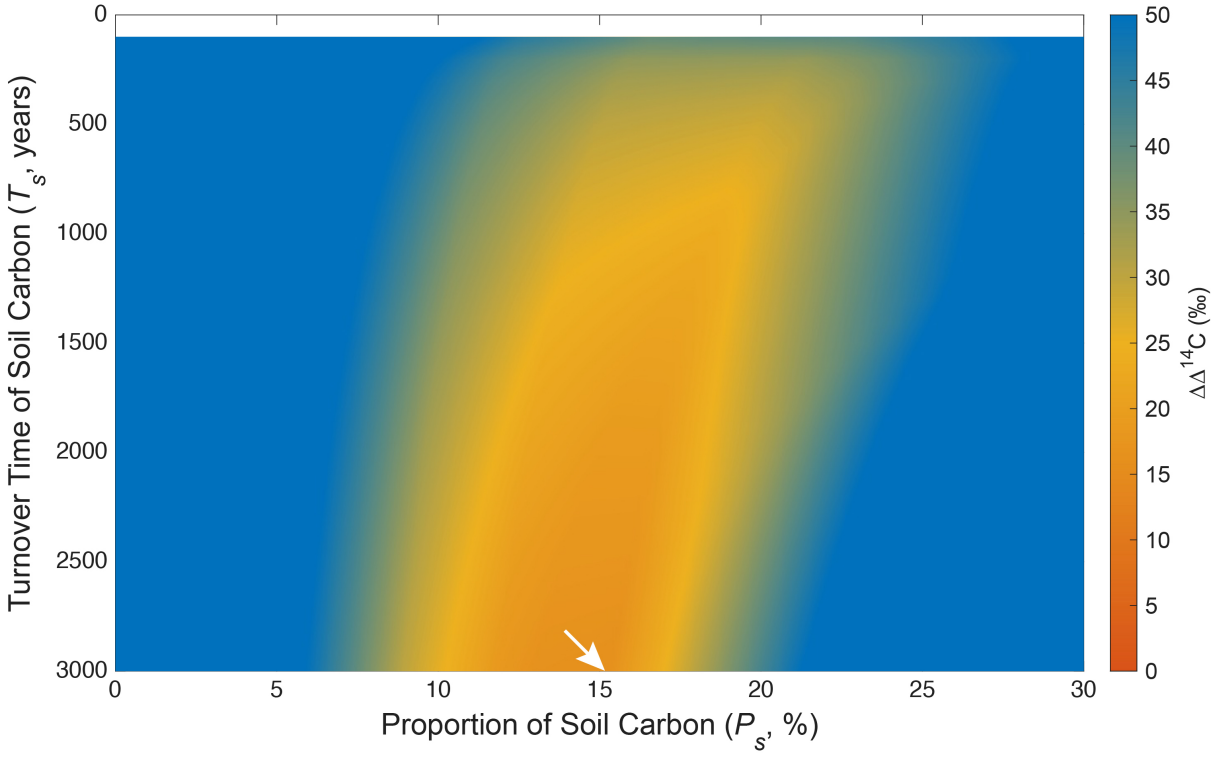

Figure S20. The $\Delta\Delta^{14}C$ heatmap that overlayed all the eight heatmaps in Figure S19. The arithmetic mean of the $\Delta\Delta^{14}C$ values from the eight years are shown. The white arrow denotes the smallest $\Delta\Delta^{14}C$ value (i.e., the most plausible model).

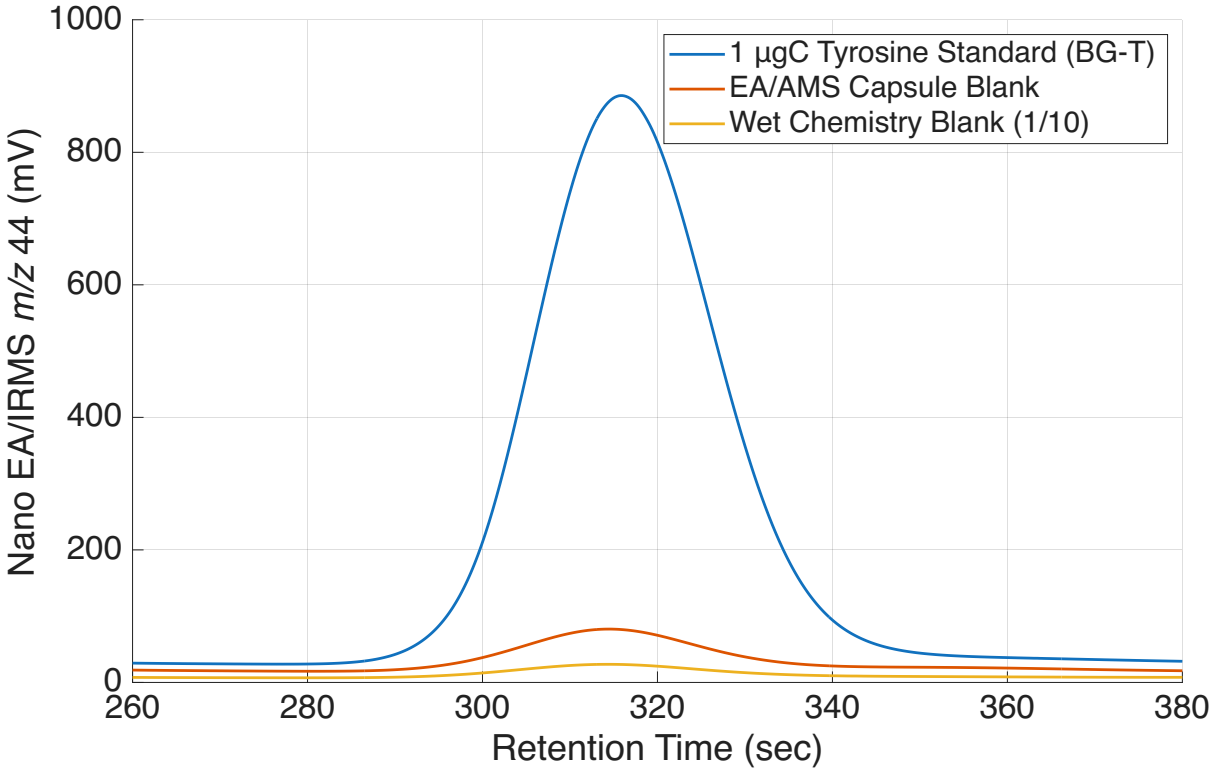

Figure S21. The Faraday cup 2 (*m/z* 44, CO_2) peaks for 1 µgC working standard, AMS tin capsule, and procedural blank (ten times diluted) on overlaid nano-EA/IRMS chromatograms.

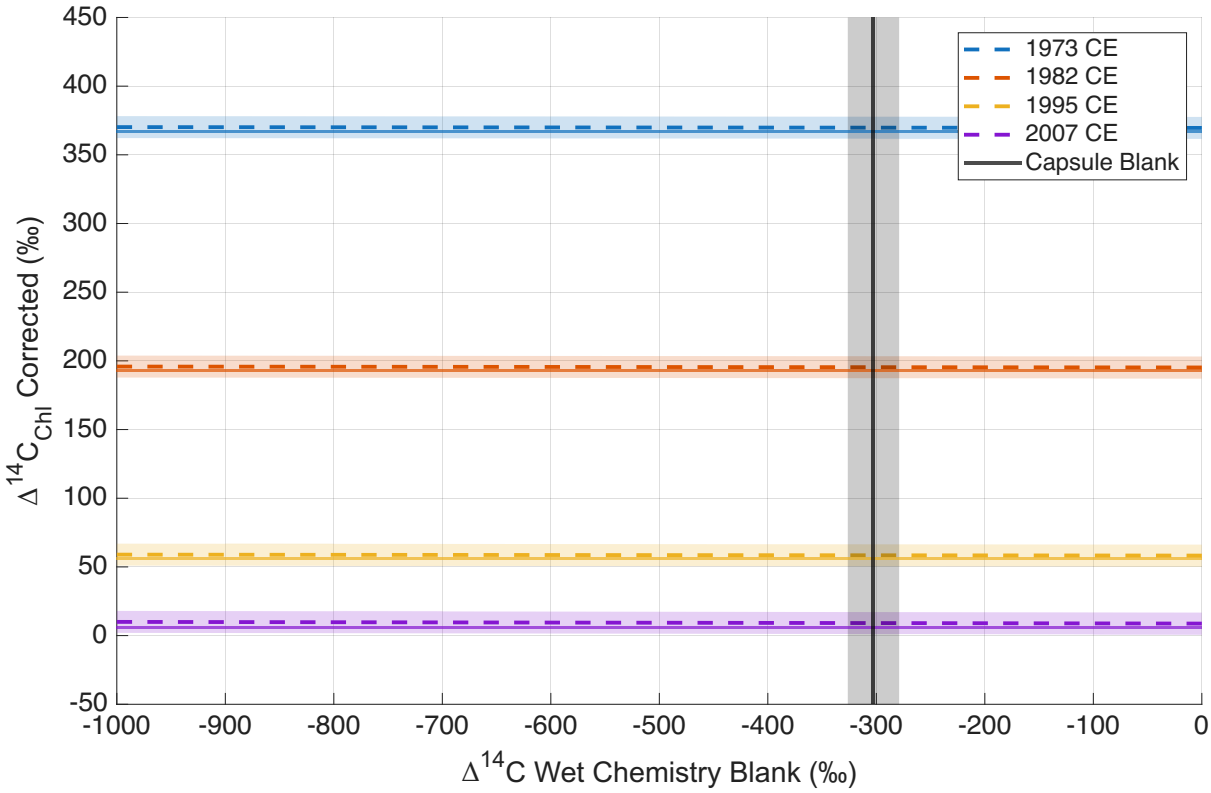

Figure S22. The effect of wet chemistry blank $\Delta^{14}C$ on the corrected $\Delta^{14}C_{Chl}$ values of the four Chl *a* data that satisfied the purity criterion and are used for modelling (1973, 1982, 1995, and 2007 CE, solid horizontal lines). Dashed lines represent the corrected $\Delta^{14}C_{Chl}$ value as a function of the wet chemistry blank $\Delta^{14}C$ (from –1,000 to 0‰) with the MICADAS analytical error (± 8‰, 1σ). The black vertical line and shading denote the AMS capsule and machine blank $\Delta^{14}C$ (–303 ± 24‰).

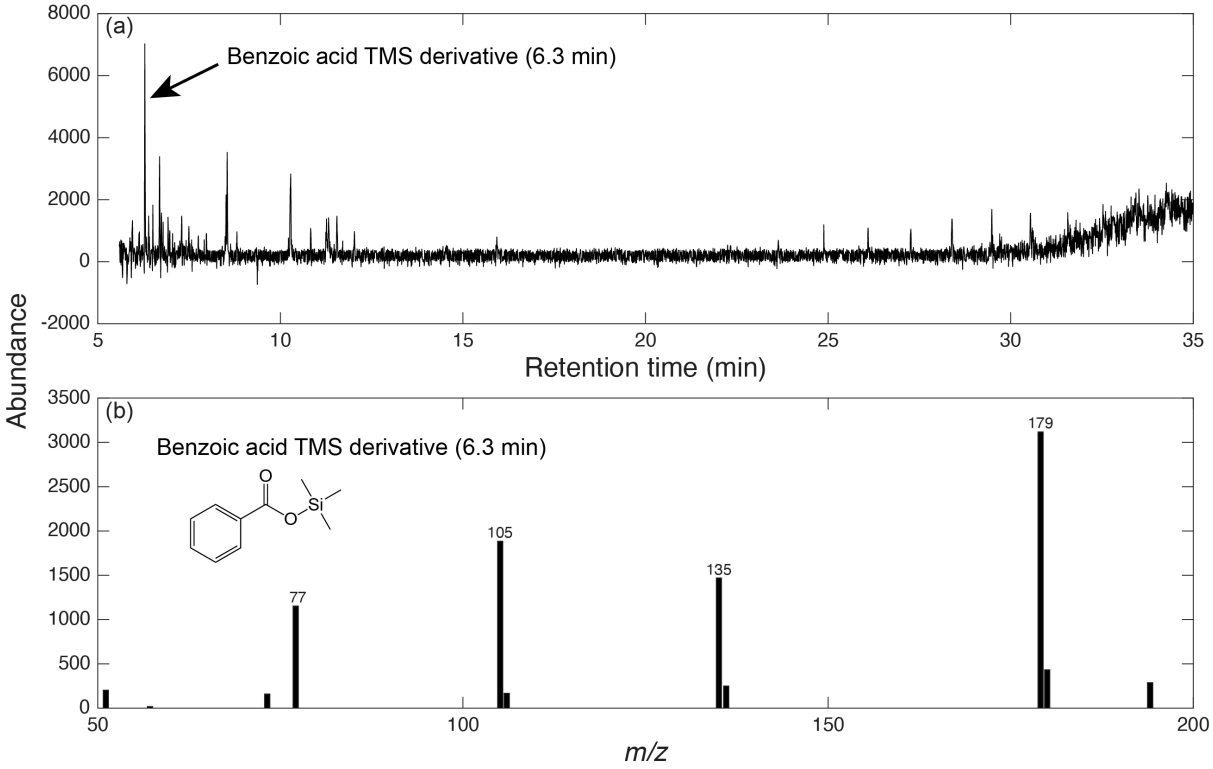

Figure S23. (a) Total ion chromatogram of the procedural blank (TMS reagent background subtracted) and (b) mass spectrum of benzoic acid TMS derivative (6.3 min).

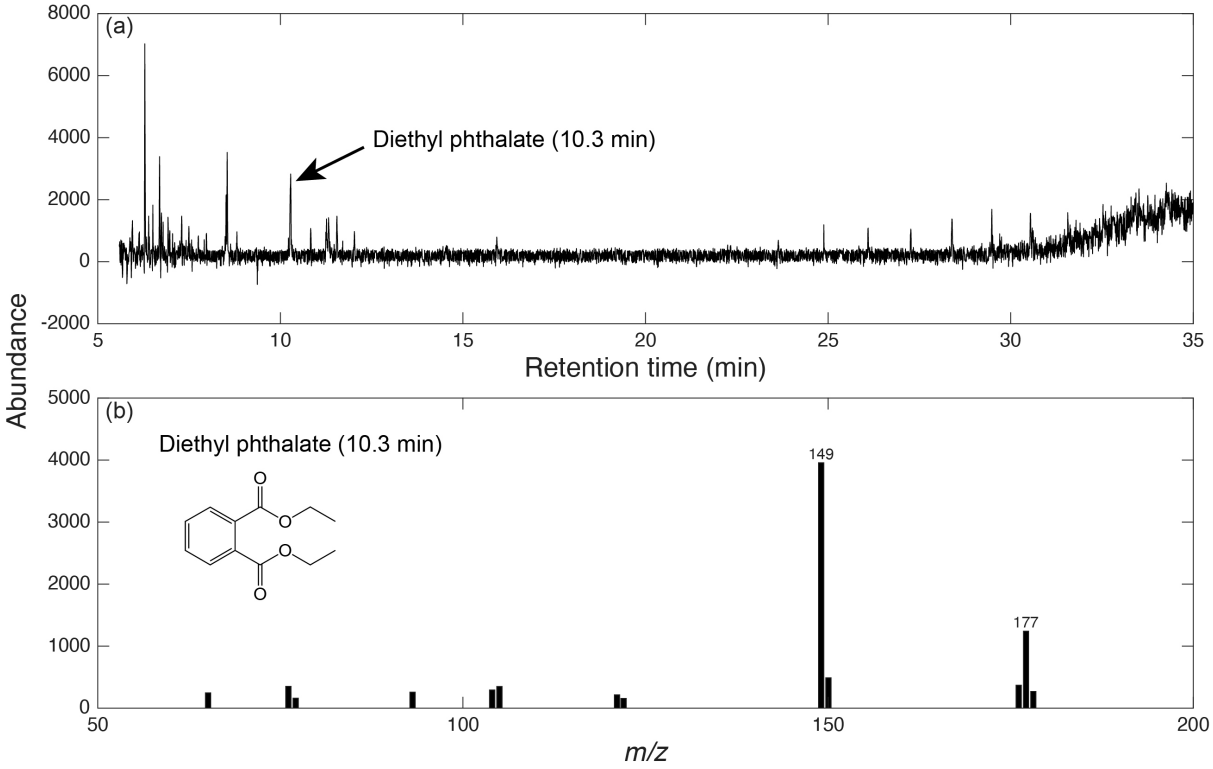

Figure S24. (a) Total ion chromatogram of the procedural blank (TMS reagent background subtracted) and (b) mass spectrum of diethyl phthalate (10.3 min).

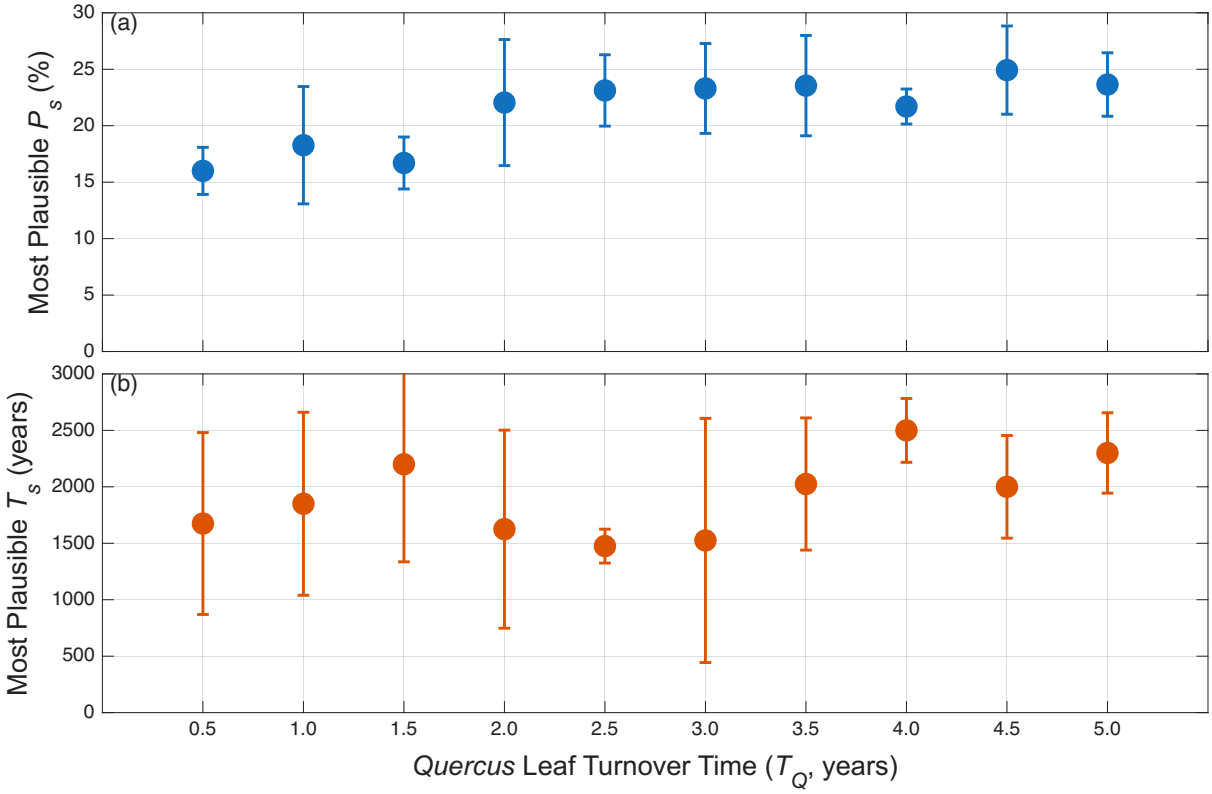

Figure S25. Sensitivity analysis of the two-pool mixing model for the change in its two outputs; the most plausible (a) proportion of soil carbon P_S and (b) turnover time of soil carbon T_S in response to the change in *Quercus* leaf turnover time T_Q values from 0.5 to 5.0 years. Mean and standard deviation of 1973, 1982, 1995, and 2007 data are shown.